N-15 photo-CIDNP MAS NMR on both photosystems and magnetic field-dependent C-13 photo-CIDNP MAS NMR in photosystem II of the diatom Phaeodactylum tricornutum

Zill, J.C.; Kansy, M.; Goss, R.; Alia, A.; Wilhelm, C.; Matysik, J.

^{15}N photo-CIDNP MAS NMR on both Photosystems and magnetic field dependent ^{13}C photo-CIDNP MAS NMR in Photosystem II of the diatom *Phaeodactylum tricornutum*

*Jeremias C. Zill,[†] Marcel Kansy,[‡] Reimund Goss,[‡] A. Alia,[§] Christian Wilhelm,[‡] Jörg Matysik[†]**

[†] University of Leipzig, Institute of Analytical Chemistry, Johannisallee 29, D-04103 Leipzig, Germany

[‡] University of Leipzig, Institute of Biology, Johannisallee 21-23, D-04103 Leipzig, Germany

[§] University of Leiden, Leiden Institute of Chemistry, Einsteinweg 55, P.O. Box 9502, 2300 RA Leiden, The Netherlands; and University of Leipzig, Institute of Medical Physics and Biophysics, Härtelstr. 16-18, D-04107 Leipzig, Germany

KEYWORDS: Photosynthesis, diatoms, *Phaeodactylum tricornutum*, Photo-CIDNP MAS NMR.

ABSTRACT: Diatoms contribute about 20-25% to the global marine productivity and are successful autotrophic players in all aquatic ecosystems, which raises the question whether this performance is caused by differences in their photosynthetic apparatus. Photo-CIDNP MAS NMR presents a unique tool to obtain insights into the reaction centers of photosystems (PS), by

selective enhancement of NMR signals from both, the electron donor and the primary electron acceptor molecules. Here, we present the first observation of the solid-state photo-CIDNP effect in the pennate diatoms. In comparison to plant PSs, similar spectral patterns have been observed for PS I at 9.4 T and PS II at 4.7 T in the PSs of *Phaeodactylum tricornutum*. Studies at different magnetic fields reveal a surprising sign change of the ^{13}C photo-CIDNP MAS NMR signals indicating an alternative arrangement of cofactors which allows to quench the Chl *a* donor triplet state in contrast to the situation in plant PS II. This unusual quenching mechanism is related to a carotenoid molecule in close vicinity to the Chl *a* donor. In addition to the photo-CIDNP MAS NMR signals arising from the donor and the primary electron acceptor cofactors, a complete set of signals of the imidazole ring ligating to the magnesium of Chl *a* can be observed.

1 Introduction

Photo-CIDNP (photochemically induced dynamic nuclear polarization) MAS NMR presents a versatile tool to investigate electronic and chemical structures of the most substantial cofactors involved in photosynthesis as well as the underlying spin dynamics (Jeschke and Matysik 2003; Daviso et al. 2008; Matysik et al. 2009; Thamarath et al. 2012; Bode et al. 2013; Najdanova et al. 2015). This technique allows for the selective enhancement of NMR signals from the donor and the primary electron acceptor molecules in photosynthetic reaction centers (RCs). The light-induced NMR intensities correlate to the local electron spin densities of the electron donor and the primary electron acceptor (Jeschke and Matysik 2003; Daviso et al. 2008; Diller et al. 2007b; Daviso et al. 2009).) Furthermore, it has been shown that the presence of carotenoids in the vicinity of the donor Chl *a* allows for quenching molecular triplet states, an effect which can

change the sign of the observed NMR signals of the donor nearby (Daviso et al. 2008; Prakash et al. 2005a; Prakash et al. 2006; Thamarath et al. 2012).

For the photo-CIDNP effect in the solid state, up to three mechanisms have been discovered to contribute to the spin-hyperpolarisation (Scheme 1): the three spin mixing (TSM), the differential decay (DD) and the differential-relaxation (DR) mechanisms (Jeschke 1998; McDermott et al. 1998; Polenova and McDermott 1999; Prakash et al. 2006; Sosnovsky et al. 2016). Under typical conditions in bacterial RCs of *Rhodobacter (R.) sphaeroides*, the TSM mechanism leads to emissive NMR signals reaching their maximum if a matching of the nuclear Zeeman frequency with the coupling of two electron spins as a spin-correlated radical pair (SCRP) and the anisotropic hyperfine coupling with a nucleus occurs (Jeschke 1998). For the DD mechanism, anisotropic hyperfine coupling is also required to build up nuclear spin polarisation from electron spin polarisation. Due to different life-times of the singlet and the triplet states of the SCRP, nuclear spin polarisation is formed, yielding in absorptive signals (Polenova and McDermott 1999). The DR mechanism occurs if the donor triplet life-time is sufficiently long, for example by absence of a near-by carotenoid, to quench nuclear polarization in the donor on the triplet pathway. As a result nuclear polarisation from the singlet pathway only remains. This mechanism occurs in both liquid and solid state. Hence, the observed signals occur selectively from the donor and have a positive sign (McDermott et al. 1998). It was shown that in quinone-blocked bacterial RC of *R. sphaeroides* wildtype, where the donor triplet life-time is 100 ns, the DR does not occur. In the carotenoidless mutant R26 of *R. sphaeroides,* the triplet is not quenched by carotenoids, hence the life-time of the donor triplet state is 100 μs (Shuvalov and Parson 1981) and strong polarization from DR is observed (Prakash et al. 2006).

The solid-state photo-CIDNP effect has already been observed in ten species (Fig. 1, for detailed taxonomic overview, see Ref. (Armbrust 2009)). Nine of them belong to either the plant or the bacterial kingdom. Recently, the effect has been demonstrated on the tenth organism that the effect can be observed in all three phototrophic kingdoms including the kingdom of chromista (Zill 2017a). The omnipresence of the effect lead to speculations about possible functional relevance (Matysik et al. 2009, Cespedes Camacho & Matysik 2014). Chromista comprise the heterokonts (or stramenopila) which include the phylum Bacillariophyta (diatoms). Diatoms are unicellular eukaryotic algae that live either as single cells or in colonies (Sumper and Brunner 2008). It is estimated that diatoms contribute about 20-25% to the global net primary biomass production (Werner 1977) which might be due to special physiological features of the diatoms like, e.g., the presence of a urea cycle (Bowler and Allen 2008; Armbrust et al. 2004; Wilhelm et al. 2006) that is even connected to their citric acid cycle. This anaplerotic function is one of the reasons why diatoms can recover shortly after a low nutrient period (Allen et al. 2011). Diatoms are also known to outcompete other organisms in turbulent waters with rapid changes of the light climate, i.e. light intensity and quality. These conditions require a high flexibility of the photosynthetic apparatus and a large photoprotective potential. The main photoprotective mechanism of diatoms is the so-called non-photochemical quenching (NPQ), which leads to the dissipation of excessive excitation energy as heat in the light-harvesting antenna of photosystem II (for reviews see Lavaud and Goss 2014 and Goss and Lepetit 2015). In addition to their high capacity for NPQ, diatoms are characterized by the presence of different alternative electron pathways which further reduce the risk of an over-excitation of the photosynthetic apparatus. These pathways include the Mehler reaction and cyclic electron

transport around PSI (Grouneva et al. 2009). Interestingly, diatoms contain an additional cyclic electron transport around PSII (Lavaud et al. 2002, Wagner et al. 2016).

Like the higher plants (embryophyta), diatoms comprise the two photosystems (PS): PS I and PS II. Photosystems are pigment-protein complexes that convert light energy into chemical energy incepted by a light-induced electron transfer. Chlorophyll dimers, i.e. pairs of chlorophyll molecules termed P_{680} in PSII and P_{700} in PSI, act as primary electron donor molecules (for a review, see Allen and Williams 1998). As a type-I RC, PS I utilizes iron-sulphur clusters as terminal electron acceptor, whereas type-II RCs like PS II use quinone molecules for this purpose. PS I has a strong reductive force, in contrast to PS II which has an oxidative force high enough to split water. The main protein subunits of PS I and PS II are highly conserved for eukaryotic phototrophic species, among others the diatoms, as well as for cyanobacteria (Barber 2006; Green and Durnford 1996; Lepetit 2010). PS I contains 19 protein subunits including PsaA (82 kDa) and PsaB (83 kDa) (Amunts and Nelson 2008) which bind the reaction center pigments including chlorophyll *a* (Chl *a*) as electron donor and four additional Chl *a* molecules in the electron transfer chain as well as three iron-sulphur clusters (Amunts et al. 2007; Ben-Shem et al. 2003; Jensen et al. 2007; Jordan et al. 2006). Beside several small protein subunits the PS II core complex comprises four main units: PsbA, PsbB, PsbC, PsbD (Dekker and Boekema 2005). PsbA and PsbD, also called D1 and D2, form the RC that binds six Chl *a*, two pheophytin *a* (Phe *a*) and two β-carotene molecules (Barber 2006; Ferreira et al. 2004; Loll et al. 2005). One of these Chl *a* molecules forms the electron donor and in contrast to PS I the primary electron acceptor is Phe *a*. PsbB and PsbC, also called CP47 and CP 43 work as inner antenna of the PS II. Together CP47 and CP43 bind about 30-40 Chl *a* and 8-10 β–carotene molecules, the number of Chl *a* and β–carotene molecules seems to be slightly higher for CP47(Barber 2006;

Ferreira et al. 2004; Guskov et al. 2009; Loll et al. 2005). The core proteins of PSI, PsaA and PsaB, are integrated into the thylakoid membrane with eleven trans-membrane helices each, in PSII the reaction center proteins D1 and D2 comprise five helices, whereas the inner antenna proteins CP43 and CP47 contain six trans-membrane helices (Schubert et al. 1998). PS I and PS II are heterogeneously distributed in green plants which means that PS I is mainly found in the stroma thylakoids and the majority of PS II is more located in the grana thylakoids (Dekker and Boekema 2005). In contrast to higher plants, diatom thylakoids are arranged in stacks of three (Gibbs 1962; Gibbs 1970; Pyszniak and Gibbs 1992). Recent results have shown that, despite the more regular thylakoid arrangement, the PSI and PSII reaction centers are organized in separated membrane domains with some interconnections to optimize photosynthesis (Flori et al. 2017).

Comprised of silicified cell walls diatoms have become interesting for microscopy for their impressive variety of shapes. Together with radiolaria and silicoflagellates, diatoms require high amounts of silica, approximately as much as nitrogen (Tréguer et al. 1995, Smetacek 1999). Hence, diatoms are model organisms for biomineralization (Wisser et al. 2015). Diatoms live nearly equally distributed in marine and limnic habitats. Since some oceanic areas, like the southern ocean and the equatorial and the subarctic pacific, are iron limited, many phototrophic organisms can hardly survive even though the regions are often rich in other nutrients. Some diatoms can adapt to low iron concentration in these high macronutrient low chlorophyll (HNLC) areas, nevertheless, a decrease of the number and the size of the chloroplasts might be a result (Lommer et al. 2012). Iron has a key function for photosynthesis since it is required in PS I, e.g. in the iron-sulphur-clusters working as terminal electron acceptors (Lommer et al. 2012). For instance *Cyclotella* (*C.*) *meneghiniana* lives rather coastal whereas *Phaeodactylum*

(*P.*) *tricornutum* (Figure 2) is more likely to grow in oceanic regions (Sayers et al. 2009; Benson et al. 2009). *P. tricornutum* can even acclimate to iron-depletion and iron-repletion (Allen et al. 2011; Kustka et al. 2007) . For diatoms living in regions far from the coast the PS II/PS I ratio has been reported to be five times higher than for coastal diatoms which was explained by the depletion of iron (Strzepek and Harrison 2004). Interestingly, a very recent study has shown that the optical properties of the frustule valves in water affect light-harvesting and photosynthesis in living diatom cells (Goessling et al. 2018). By photon trapping and forward scattering of blue light they facilitate light redistribution and photosynthesis in cell areas distant from the directly illuminated area. It is assumed that the photonic structures of the diatom cell walls support the ecological success of the diatoms.

Based on their size and the number of plastids diatoms were initially divided into one pennate class (latter referred to as Bacillariophyceae), whose members are up to a few μm large and have only one chloroplast and one centric class comprising species which can reach a few millimeters in diameter and which can have a few plastids (Smetacek 2000). Today the centric forms are divided into two classes: Coscinodiscophyceae and Mediophyceae. The diatom for which the solid-state photo-CIDNP effect has been shown before, *Cyclotella meneghiniana*, belongs to the latter class (Zill et al. 2017b). It is assumed that there are up to 200,000 species in the diatom phylum, making them the most speciose algae (Mann and Droop 1996). Whole genome sequences have been published for two diatom species: *Thalassiosira pseudonana* from the Mediophyceae class and *P. tricornutum* from the Bacillariophycea class. It was shown, that these two organisms have only around 55% similarity on the genomic level (Bowler and Allen 2008). This surprisingly small similarity leads to the question to what extent the photosynthetic machineries are comparable in both diatom classes. Recently, the genome sequence of the cold-

adapted diatom *Fragilariopsis cylindrus* has been published and compared to the genomes of the temperate diatoms mentioned above (Mock et al. 2017).

In the present study, we aim to investigate whether the solid-state photo-CIDNP effect can also be observed in the Mediophyceae class of diatoms, using the species *P. tricornutum*. Since the effect is assumed to be an inherent property of all photosynthetic RCs, it has been suggested that the related spin-dynamics is of functional relevance for photosynthesis (Matysik et al. 2009; Céspedes-Camacho and Matysik 2014). The growing number of species on which the effect can be observed supports this idea. The study also will reveal information about the intactness of the extracted PSs. Despite the complete absence of x-ray structures of diatom photosynthetic RCs, it is expected, but not proven, that the cofactors as well as their arrangement in the RC are similar for PSs in both the chromista and the plantae kingdoms (Barber 2006; Green and Durnford 1996). Photo-CIDNP MAS NMR can provide information about the chemical identity of the electron donor and the primary electron acceptor as well as about the presence of carotenoid molecules nearby. Since the solid-state photo-CIDNP effect has been demonstrated for PS I of an example from the Bacillariophyta, we focus on PS II in this work and reveal potential similarities and differences between diatoms and green plants.

2 Materials and Methods

2.1 Sample Preparation

Preparation of uniformly ^{15}N-labeled thylakoid membranes and a combined PSI and PSII fraction from *P. tricornutum*

The diatom *P. tricornutum* was grown in artificial seawater preparation (ASP-2) (using ^{15}N-labelled KNO_3) as air-lift batch culture at 20 °C with an ambient light intensity of 50-60 μmol photons m^{-2} s^{-1} and a light-dark regime of 14/10 h.

The sample was prepared following a similar protocol as applied for a photo-CIDNP active PS I preparation from the diatom *C. meneghiniana* (Zill et al. 2017b) A detailed version of the protocol is described by Lepetit et al. 2007 Cells were harvested by centrifugation for 5 min at 1,000 *g* and resuspended in buffer A (10 mM 2-(*N*-Morpholino)ethanesulfonic acid (MES) pH 6.5, 2 mM KCl, 5 mM ethylene-diaminetetraacetic acid (EDTA), and 1 M sorbitol). Cell lysis was performed with a pre-chilled French Pressure cell (Thermo Spectronic, UK) at 12,000 psi. The French Press extract was centrifuged for 10 min at 1,000 *g* to remove cellular debris and intact cells. The supernatant was transferred in a fresh tube and thylakoids were harvested by centrifugation for 15 min at 10,000 *g*, resuspended in a small volume of buffer B (10 mM MES at pH 6.5, 2 mM KCl, 5 mM EDTA) and stored on ice in darkness until solubilisation. Thylakoid membranes were solubilized with *n*-dodecyl β-D-maltosid (β-DM)at a Chl concentration of 1 mg/mL and a detergent/Chl ratio of 20. Following solubilisation at 4 °C and dark conditions non-solubilized material was removed by centrifugation at 20,000 *g* for 10 min and the supernatant was immediately transferred on a linear sucrose density gradient (0.2-1 M sucrose in buffer B, supplemented with 0.06% β-DM) for further separation. Ultracentrifugation (Optima C-90 K with SW-28 rotor, Beckman-Coulter, USA) of the density gradients was performed at 120,000 g for 17 h at 4 °C and resulted in different bands, among them a prominent green band representing the photosystems (Fig. 3, A). Sample proteins were characterised by denaturing protein gel electrophoresis (Laemmli 1970) followed by coomassie staining (Dyballa and Metzger 2009) (Fig. 3, B (Nagao et al. 2013)).

Prior to the NMR experiment the sample was concentrated using Centricon plus 20 centrifugal filter devices (Millipore Corporation, Bedford, USA, Amicon®, 30 kDa molecular weight cutoff) for a centrifugation step at 3,500 *g* and 4 °C. The terminal electron acceptors were finally reduced by adding 1 M sodium dithionite solution to a final concentration of 100 mM in an oxygen free atmosphere, before adding the sample into a transparent 4-mm sapphire rotor.

Preparation of PS II core complexes from *P. tricornutum*

P. tricornutum was grown in artificial seawater preparation (ASP-2) at 18 °C with a light intensity of about 100 $\mu E*m^{-2}*s^{-1}$ and a light-dark regime of 14/10 h. Cell material used for sample preparation described in this section was harvested and stored in buffer A at -80 °C prior preparation. The *P. tricornutum* cell suspension was quickly thawed on ice, diluted with buffer A and transferred in a pre-chilled French-pressure cell. Preparation of PS II was performed similar to the protocol in the previous section with only minor modifications: for higher purity thylakoids were harvested at 10,000 *g*, unsolubilized material was spun down at 40,000 *g* after solubilisation and a sucrose gradient ranging from 0.1-0.6 M (0.03% β-DM) was used.

The sucrose density gradient band containing PS II was concentrated before the MAS NMR experiment using Centricon plus 20 centrifugal filter devices (Millipore Corporation, Bedford, USA, Amicon®, 30 kDa molecular weight cutoff) for centrifugation at 3,500 *g* and 4 °C. In order to reduce the quinones Q_A and Q_B acting as electron acceptor 1 M sodium dithionite solution was added to a final concentration of 100 mM in an oxygen free atmosphere.

2.2 MAS NMR measurements

MAS NMR spectroscopy was performed using a DMX-200-MHz and an Avance III 400-MHz wide-bore NMR spectrometer which were equipped with a 4-mm MAS probe (Bruker,

Karlsruhe, Germany) for MAS NMR experiments at different magnetic fields. Samples were packed into 4-mm sapphire rotors and inserted into the MAS probe. For homogeneous sample distribution against the rotor wall, the temperature was decreased slowly at a low spinning speed of about 1,000 Hz Fischer et al. 1992. Both, light and dark spectra, were collected using a Hahn-echo pulse sequence with two-pulse phase modulation (TPPM) proton decoupling (Bennett et al. 1995). ^{13}C and ^{15}N-MAS NMR spectra were collected at a temperature of 250 K with a deviation of approximately 2 K and under continuous illumination with white light using a 1,000-W xenon-arc lamp (Matysik et al. 2000). Calibration of the sample temperature was performed beforehand by measuring the melting points of different substances (distilled water, 4-decanone and 3-octanone). The correlation of the obtained corrected temperatures with ^{207}Pb chemical shift of a solid powder of lead nitrate measured at the according temperatures (Bielecki and Burum 1995; Haynes 2015; Zill 2017a) showed that the temperature difference of a sample measured at light conditions is about 1 K higher than under dark conditions. The spinning frequency was 8 kHz and the cycle delay was 4 s.

Photo-CIDNP MAS NMR experiments on PS II of *P. tricornutum*: For both spectra measured at 4.7 T, line-broadening of 20 Hz and for the spectra at 9.4 T, line broadening of 30 Hz was applied prior Fourier transformation. The same phase-correction parameters (PHC0 = -65.0° and PHC1 = -68.0° for the spectra at 4.7 T and PHC0 = 180.0° and PHC1 = -180.0° for the spectra at 9.4 T), required to properly phase the histidine spectrum (Fig. 4), were used for both the dark and photo-CIDNP MAS NMR spectra.

Photo-CIDNP MAS NMR experiments on the combined PSI and PSII fraction of *P. tricornutum*: ^{15}N-MAS NMR spectra of membranes are presented with a line broadening of 40 Hz and for the ^{13}C MAS NMR spectra a line broadening of 10 Hz was applied prior Fourier

transformation. ^{15}N-chemical shifts are given relative to liquid $^{15}NH_3$ using the amino NH_2 response of histidine•HCl at 49.09 ppm. The same phase-correction parameters (PHC0 = -180.0° and PHC1 = 0.0° for the ^{13}C MAS NMR spectra and PHC0 = 125.4° and PHC1 = 42.7° for the ^{15}N-MAS NMR spectra), required to properly phase the histidine spectrum, were used for both the dark and light photo-CIDNP MAS NMR spectra.

All ^{13}C MAS NMR spectra were referenced using the ^{13}COOH resonance of solid cationic histidine•HCl at 173.2 ppm (Li and Hong 2011).

3 Results and Discussion

3.1 ^{15}N photo-CIDNP MAS NMR spectra of the combined PSI and PSII fraction of *P. tricornutum*

Figure 5 shows the ^{15}N-MAS NMR spectra of fractions including PS I and PS II of *P. tricornutum* at a magnetic field of 9.4 T in the dark (A) and under continuous illumination with white light (B). The spectra were collected with about 45,000 scans and a cycle delay of 4 s. The characteristic ^{15}N NMR signals of a protein can be observed between 150 and 0 ppm in the dark spectrum (A). Some features below 100 ppm can be attributed to the ^{15}N in arginine and lysine residues in the protein matrix (Prakash et al. 2005b). In the light spectrum (B), additionally to the signals observed in the dark, twelve emissive (negative) and four absorptive light-induced signals can be observed. This is the first time, that the ^{15}N-solid-state photo-CIDNP effect has been shown in the taxonomic kingdom of chromista, and it is also the first time that the solid-state photo-CIDNP effect has been observed in the pennate class of diatoms (Bacillariophyceae (Fig. 1). The fact that the effect can be observed in both main classes of the

diatom phylum together with species from all other phototrophic kingdoms implies that it is indeed an inherent property of all photosynthetic systems.

3.1.1 Signal assignments of the ^{15}N photo-CIDNP MAS NMR spectra of the combined PS fraction of *P. tricornutum*

As shown below, the well-known signals of the cofactors acting as electron donor and primary electron acceptor and forming the SCRP, i.e., Chl *a* or Phe *a*, can be straightforwardly assigned to the light-induced signals reported here. An overview on the resonances enhanced by the solid-state photo-CIDNP effect together with chemical shift data from literature is given in Tab. 1. For a more detailed view on the light-induced signals, see Fig. 6. Since the sample consists of both photosystems, PS I and PS II, the light-induced signals can be retraced to four different types of cofactors: Chl *a*, which acts in PS I as both donor and primary electron acceptor, furthermore as electron donor in PS II, as well as Phe *a* acting as primary electron acceptor in PS II.

Signals attributed to PS I: The strongest signals appear between 140 and 260 ppm. The signal at 255.5 ppm can be assigned to the N-IV of the donor Chl *a* of PS I, whereas the smaller signal at 251.9 ppm might be induced from the epimer of Chl *a* in the special pair (for numbering see Fig. 7). This can only be explained by a dimeric feature of the donor. Although the P700 in PS I appears to be a structural dimer of a Chl *a* and its epimer Chl *a*', previous data have provided indication that the donor acts as a monomer with at least 85% of the electron spin density located on a single Chl *a* (Zill 2017a). This conclusion was also derived from EPR studies (Käß and Lubitz 1996; Mac et al. 1996; Deligiannakis and Rutherford 2001). A strong emissive resonance occurs at 212.0 ppm and can be conveniently assigned to the N-II in the PS I donor Chl *a*. Since this signal at 198.8 ppm has not been observed in other ^{15}N-photo-CIDNP MAS NMR spectra of a plant PS I, it cannot be finally concluded whether it has been induced by

the N-II or the N-III of the donor Chl *a*. An assignment of the resonance to the N-II would also support the idea of a donor having some electron spin density on a second cofactor. It appears that the donor nitrogens resonate at a slightly higher chemical shift than in the Chl *a* measured in solution. As shown in the literature (Thamarath et al. 2012), the donor of the bacterial RC of *R. sphaeroides* resonates at lower ppm values and must therefore be partially negatively charged. Since the gyromagnetic ratio γ of ^{15}N is negative, the opposite is the case here. Hence, the signal at 198.8 ppm might more likely be induced from the N-III of the donor Chl *a*. That would imply that the donor of PS I is also partially negatively charged. The signal at 186.0 ppm can be assigned to the N-I of the same molecule which is in good agreement with the data from the literature.

While all signals from the donor Chl *a* appear with negative sign, the signals from the acceptor in PS I are absorptive. For the Chl *a* at the acceptor site of PS I, all four resonances can be assigned in good agreement with data from literature (Diller et al. 2007a). In analogy to the donor resonances, the most deshielded signals at 233.5 ppm and 206.1 ppm can be assigned to N-IV and N-II, respectively. The signal at 193.1 ppm can be assigned to N-III, and the resonance at 190.8 can be attributed to N-I.

Hence, some of the signals observed in the combined PSI and PSII fraction can be assigned to Chl *a* positions at the PS I donor site, these are emissive, other to Chl *a* positions at the acceptor site, which are absorptive. It appears that there is not only electron spin density on one branch of the intrinsic PSI electron transport but also some amount on the other branch.

Signals attributed to PS II: The most deshielded nitrogen position of the Chl *a* or Phe *a* cofactors is N-IV. In case of the PS II donor, Chl *a* N-IV resonates at 248.5 ppm. The signal at

213.4 ppm can be assigned to N-II and the resonances at 195.9 ppm to the nitrogen in the ring III of the porphyrin structure.

In contrast to PS I, the signals from both the electron donor (Chl *a*) and primary electron acceptor (Phe *a*) occur with emissive polarisation. The signals assigned to PS II are attributed to a single Chl *a* cofactor indicating a monomeric donor. The most deshielded signal at 297.3 ppm can be assigned to the N-IV of the Phe *a* cofactor which is in good agreement with data from Chl *a* in solution (Boxer et al. 1974) and photo-CIDNP experiments performed on PS II from spinach (Diller et al. 2007a). The signal at 138.6 ppm could be assigned to N-III.

An additional resonance can be observed at 243.7 ppm. In previous Photo-CIDNP MAS NMR studies on PS II from spinach, a signal at 243.8 ppm has been assigned to the axial histidine residue close to the donor (Diller et al. 2007a). Hence, it seems reasonable to assign the resonance observed at 243.7 ppm in this work to the π-N of the axial histidine of the monomeric donor.

3.1.2 Lineshape and linewidth in the ^{15}N photo-CIDNP MAS NMR spectra of the PSI and PSII fraction of *P. tricornutum*

Besides the signals at 251.9, 193.1 and 190.8 ppm, where no specific lineshape can be determined due to the low signal-to-noise ratio, the lineshape of the other stronger and isolated signals is always Lorentzian, which means that the natural lineshape is not disturbed by any broadening effect. The light-induced signals appear with a narrow linewidth of about 40-70 Hz. Except the signal at 186.0 ppm, resonances attributed to the donor are significantly narrower (FWHM of about 40 Hz) than the acceptor signals, which resonate with a linewidth of 55-70 Hz. Both, Lorentzian lineshape and the narrow linewidth indicate a rigid donor and a more flexible

acceptor. Such a lineshape and -width has also been observed in plant PSs (Fischer et al. 1992; Alia et al. 2004; Diller et al. 2007b). This allows to conclude that in the diatom PSs the electron transfer occurs in a rigid matrix.

3.1.3 Comparison of the ^{15}N spectra of *P. tricornutum* with those of other species

Signals assigned to cofactors in PS I: The observed signals have been assigned in comparison to data obtained from PS I and PS II from spinach (Diller et al. 2007b) (Table 1). Since *P. tricornutum* is an eukaryotic organism, comparing the PSs of diatoms with those of eukaryotic plants like spinach or duckweed appears very appropriate, as their PSs are assumed to be highly conserved (Barber 2006; Green and Durnford 1996). Indeed, the similarities between the light-induced spectrum of *P. tricornutum* and the spectra of PS I and PS II from spinach are obvious in the present work. Interestingly, the spectrum of the diatom reveals an additional weak signal at 224.9 ppm which has been assigned to the τ-N of the axial histidine of the monomeric donor Chl *a*. A comparable additional signal has not been reported from the photo-CIDNP MAS NMR spectra of spinach.

The ^{15}N photo-CIDNP MAS NMR spectra from PS I of duckweed (*Spirodela oligorrhiza*) (Janssen et al. 2012) and spinach are very similar but three more signals occur in the earlier one. These signals at 191.0, 210.0 and 253.0 ppm have been assigned to N-III, N-II and N-IV of the donor Chl *a*. The absorptive resonance at 210.0 ppm, together with a signal at 206.3 ppm, has been attributed to the N-II of Chl *a* acting as the primary electron acceptor. This has been explained (Janssen et al. 2012) as a result of both electron transport branches being active in PS I. The third additional signal at 253.0 ppm also indicated the presence of electron spin density on both branches (Janssen et al. 2012). In the spectrum of PS I from duckweed, the N-III of the donor resonates as a clearly emissive signal at 191.0 ppm, whereas in the spectrum of spinach the

absorptive N-I signal of the primary electron acceptor is found at almost the same position (190.9 ppm). It is remarkable that in the present work on *P. tricornutum*, the signal at this chemical shift is absorptive but nearly lost in the noise. Hence, it might be possible that a second N-III donor signal quenches a part of the observed polarisation in this spectral area.

Furthermore, the overall pattern of the PS I spectra of spinach and duckweed differs significantly. Besides the mentioned change of the sign of the signal at about 191 ppm, the strongest emissive resonances at 211.4 and 254.3 ppm are much stronger in the spectrum of duckweed. In contrast, the two most prominent absorptive signals at 206.3 and 233.4 ppm are more noticeable in the spectrum of spinach. It appears that in the spectrum of *P. tricornutum* both emissive and absorptive signals are rather strong. In addition, the N-IV donor signals (255.5 ppm and 251.9 ppm) and also the signals attributed to histidine (243.7 ppm and 224.9 ppm) are stronger than in the spectra of spinach and duckweed. The spectrum of *P. tricornutum* reveals electron spin density more equally distributed on the electron donor and acceptor as well as on the ligating histidine, compared to the spectra of duckweed and spinach. In any case, the highest electron spin densities can be observed on N-II and N-IV for *P. tricornutum* (for an electron spin density map see Fig. 7) as well as for duckweed (Diller et al. 2007b; Janssen et al. 2012). In contrast, electron spin density decreases from N-II to N-I to N-IV and finally to N-III in the case of spinach. This was not observed in the diatom spectrum recorded in the present study (Janssen et al. 2012).

Signals assigned to cofactors in PS II: The resonances observed from PS II in the photo-CIDNP MAS NMR spectrum of membranes of *P. tricornutum* are comparable in terms of the chemical shifts and the corresponding intensities to the PS II spectrum of spinach observed at the same magnetic field (Diller et al. 2007b).

The conclusion drawn from the presented light-induced spectrum are in-line with the previous assumption (Barber 2006; Green and Durnford 1996; Lepetit 2010) that Chl *a* acts as electron donor in both PSs and also as primary electron acceptor in PS I and Phe *a* functions as primary electron acceptor in PS II like in higher plants.

A depicted electron spin density pattern of PS II, reflecting the local electron spin density, is presented in Fig. 7. In contrast to the pattern of PS I, no hyperpolarization can be observed on N-I. Comparison to the pattern observed on PS II from spinach (Diller et al. 2007b) reveals great similarity, except for N-II, which shows a higher electron spin density in the case of *P. tricornutum*.

Comparison of the electronic structures of PS I and PS II from *P. tricornutum*: The data of the diatom *P. tricornutum* obtained with ^{15}N photo-CIDNP MAS NMR reveal similar electronic structures of the radical pairs in both PSs as in higher plants. The electron spin density distribution in the donor of PS I appears slightly distinct for different eukaryotic PS I preparations: while in PS I of spinach the highest electron spin density has been observed on the N of ring II, it is more equally distributed on N-II and N-IV in *P. tricornutum*. This is similar to the situation in duckweed (Janssen et al. 2012). Hence, this ^{15}N photo-CIDNP MAS NMR analysis might suggest that the difference between PS I and PS II of higher plants is more pronounced than the differences between the two PSs of diatoms.

3.2 ^{13}C photo-CIDNP MAS NMR spectra of the combined PSI and PSII fraction of *P. tricornutum*

The ^{13}C MAS NMR spectra of the PSI/PSII fraction of *P. tricornutum* in the dark (A) and under continuous illumination (B) have been detected at 9.4 T (Fig. 8). The spectra were collected over 3 days with a number of scans of about 65,000 and a cycle delay of 4 s.

Between 0 and 100 ppm, the characteristic signals of a protein can be observed together with twelve sharp signals which arise from sucrose that was present in the buffer due to the isolation in a sucrose density gradient (see 2.1). A set of broad signals can be observed between 128.5 and 130.2 ppm which are probably induced by the aromatic side chains of the proteins. The signal at 172.7 ppm is most likely due to carbonyl carbons of the amino acids. Additionally, in the light spectrum (see below), a number of 16 emissive light-induced signals and two absorptive light-induced signals can be identified. The predominance of negative signals is not surprising, since the solid-state photo-CIDNP effect has been shown to be more efficient at this field in case of PS I (Roy et al. 2007a). In contrast to PS II preparations from higher plants, negative signals can also be observed in PS II of *P. tricornutum* (Roy et al. 2007a). This is the first-time report of the ^{13}C solid-state photo-CIDNP effect in this taxonomic class (Bacillariophyceae, Fig. 1).

3.2.1 Signal assignments of the ^{13}C photo-CIDNP MAS NMR spectra of the PSI/PSII fraction of *P. tricornutum*

Table 2 compiles the light-induced ^{13}C chemical shifts observed on the PSI/PSII fraction the sucrose gradient fraction of *P. tricornutum* comprising both PSs and compares them to literature data. Since the solid-state photo-CIDNP effect selectively enhances the cofactors acting as electron donor and as primary electron acceptor, a signal might be induced by one of four possible molecules if also in PS I only one branch of intrinsic electron transport is active.

An assignment to a donor or acceptor position on the basis of the *sign* of the signal is not straightforward in ^{13}C photo-CIDNP MAS NMR experiments. In any case, many signals can be reasonably assigned by their well-known *frequency* to either a Chl *a* or a Phe *a* cofactor. The latter one acts as primary electron acceptor in PS II as mentioned above. The assignment of the enormous number of carbon positions to the observed signals appears to be a more puzzling

issue for Chl *a*. Since the electron donor is known to be rigid (Fischer et al. 1992), signals which are relatively broad might more probably be assigned to the primary electron acceptor, rather than to the donor. Another hint might be given by the intensity of a signal, since the presented spectra have been observed at 9.4 T, where PS I shows the highest photo-CIDNP induced polarisation, in contrast to PS II where the solid-state photo-CIDNP effect has been observed at a magnetic field of 4.7 T (Roy et al. 2007a).

A detailed view on the light-induced resonances is given in Fig. 9. The most deshielded signal appears emissively at 192.1 ppm and can be assigned to a carbon at the 13^1-position of Chl *a*. The signal resonates at the same position like a donor Chl *a* observed in PS I of the diatom *C. meneghiniana* (Zill et al. 2017b) and the signal is also observed in PS II of *P. tricornutum* (see chapter 3.3.1), which does not allow to assign this signal to a specific cofactor. The emissive resonance at 168.3 ppm can be assigned to a C-19 position and is most suitable for a Chl *a* cofactor. Since the signal appears rather narrrow (52 Hz) it is probably induced by a donor Chl *a*. The broad (124 Hz) signal at 161.6 ppm can be caused by both: a C-14 of a Chl *a* and a C-16 of a Phe *a* cofactor. It appears reasonable to assign the signal at 156.3 ppm to Chl *a* C-1 position. The emissive signals at 154.7 and 153.8 ppm can be conveniently assigned to atoms at the C-6 position of Chl *a* or Phe *a* of PS II, however with opposite sign compared to the literature (Diller et al. 2005; Janssen 2013). Hence, these signals are most probable induced by Chl *a* and Phe *a* of PS II. The absorptive signal at 152.7 ppm can conveniently be assigned to a C-16 of the donor (Chl *a*) in PS II since the signal has not been observed in PS I preparations and this position in Phe *a* resonates around 161 ppm. The carbons 4 and 14 of Phe *a* can be observed at the same position at 151.1 ppm.

The strongest emissive light-induced resonance is found at 148.5 ppm and might be induced by a carbon of a Chl *a* at the C-4 position. Comparison with the literature implies that this Chl *a* is very likely the donor in PS II. The emissive signal at 147.7 ppm appears to resonate from C-9 or C-11 of a Chl *a*. Probably, the emissive signal at 145.6 ppm resonates due to a C-8 of a Chl *a* or a Phe *a* cofactor. Another absorptive resonance at 143.3 ppm can be assigned to the C-1 position of a Phe *a*. The small resonance at 142.5 ppm cannot be assigned to a cofactor. It might be induced by the protein. Both signals at 139.9 ppm and 137.3 ppm might be induced from a donor or acceptor C-3 or from the C-2 position of Chl *a*, respectively. The latter signal can also be assigned to the ε-position of a histidine close to the donor in PS II. The emissive signal at 133.4 ppm can be assigned to the C-7 position of a Chl *a* cofactor or the γ-C of histidine. Another resonance that is attributed to the δ-C of histidine can be observed at 118.2 ppm. The resonance at 106.3 ppm might appear from a C-10 or C-15 of a Chl *a* or Phe *a* cofactor. The most shielded light-induced signal arises from the C-5 methine carbon of Chl *a*.

According to literature data (Diller et al. 2005; Janssen 2013; Zill et al. 2017b), PS I is expected to be predominant over PS II at this magnetic field. In the present spectra, out of the 18 light-induced resonances, at least twelve cannot be assigned to cofactors of a specific PS. Signals assigned to Phe *a* must originate only from PS II. Some of these even show emissive polarisation, which is not expected from PS II in this chemical shift region (for a more detailed discussion see chapter 3.3.2). The assignment of some signals to Chl *a* of PS II is clearly indicated. Hence, the ^{13}C photo-CIDNP MAS NMR spectra of membranes of *P. tricornutum* reveal resonances from both PSs.

3.2.2 Comparison of the spectrum of the PSI/PSII fraction of *P. tricornutum* with spectra from PS I and II of other species

The most apparent difference between photo-CIDNP MAS NMR spectra of plant PS I and PS II is the pattern of signs. For PS I the entirely emissive pattern has been explained by a predominance of the TSM mechanism over the DD mechanism. A different situation has been reported for PS II which is expressed in the positive set of signals in the aromatic range, caused by the additional action of the DR on the donor, combined with negative signals from the methine carbons (Diller et al. 2005) Hence, for the membrane preparation presented here both, positive and negative signals, would be expected. In any case, in this work only one absorptive signal at 152.7 ppm can be assigned to a Chl *a* cofactor and one absorptive resonance is likely to be induced from Phe *a* (C-1 at 143.3 ppm). All other signals are emissive. Even though for PS II, the magnetic field optimum for the observation of the solid-state photo-CIDNP effect is at lower field at least some signals from PS II with positive sign are expected. The spectrum presented in Fig. 9 does not show a mixed pattern of emissive and absorptive signals as expected from previous works (Diller et al. 2005; Janssen 2013) on plant PSs. In contrast, for at least two signals (C-6 of Chl *a* at 154.7 pm and C-6 of Phe *a* at 143.3 ppm) a clear inversion of the sign is observed. Hence, signals from PS II can be observed but with opposite sign. To explore the origin of the sign change, a sample enriched with PS II is investigated in chapter 3.3 of this work.

3.3 Magnetic field dependent ^{13}C Photo-CIDNP MAS NMR spectra of PS II from *P. tricornutum*

The ^{13}C MAS NMR spectra of PS II core complexes from *P. tricornutum* at magnetic fields of 4.7 T (A and B) and 9.4 T (C and D) in the dark (A and C) as well as under continuous illumination (B and D) are shown in Fig. 10. All spectra have been recorded over three days with a number of scans of about 64,000. The characteristic ^{13}C NMR signals of a solid protein arise

between 0 and 100 ppm from the C-α amino acids of the protein backbone. The sharp response at 104.3 ppm might be due to sucrose or 2-(N-morpholino)ethanesulfonic acid which were both present in the buffer due to the isolation procedure. In addition, a number of light-induced signals occurs upon illumination at both magnetic fields (Fig. 10, spectrum B and D). Hence, the first observation of the solid-state photo-CIDNP effect in PS II extracted from a diatom is reported in this study.

3.3.1 Signal assignments of the ^{13}C photo-CIDNP MAS NMR spectra of PS II from *P. tricornutum*

200 MHz NMR spectrum: A detailed view on the enhanced resonances at 4.7 T is presented in Fig. 11, spectrum A. A number of eight absorptive and two emissive signals occur upon illumination. The absorptive signal at 168.4 ppm is most probably induced by a C-19 of either a Chl *a* or a Phe *a* cofactor. However, an assignment to Chl *a* seems more likely since the chemical shift fits better to the one observed from Chl *a* in solution and the lineshape is very narrow (FWHM of 43 Hz), which is typical for the usually more rigid donor. The resonance at 162.4 ppm can conveniently be assigned to the C-14 of the Chl *a* cofactor. For this signal also a narrow line-width of 49 Hz is observed. The signal at 156.0 ppm seems to have a shoulder, most probably due to two overlapping signals. It might be caused by the C-1of the Chl *a* cofactor. The shoulder of the signal might be the C-6 of the Phe *a* cofactor. The absorptive signal at 152.1 ppm can be assigned to the C-16 of the Chl *a* acceptor in good agreement with literature data (Diller et al. 2005; Janssen 2013). This is also supported by the line-width of about 55 Hz. The weak resonance at 149.5 ppm might be due to the C-4 of Chl *a*. Another weak signal at 148.7 ppm could be induced from C-9 or C-11 of Chl *a*. The strongest signal arises at 147.0 ppm and can also be attributed to both, C-9 and C-11 of the Chl *a* donor, which is supported by the rather

broad line-width of about 90 Hz (FWHM). Another weak resonance can be observed at 133.1 ppm and might be assigned to either the C-7 of Chl *a* or a position in the histidine residue coordinating to the Chl *a* donor molecule. The only emissive signal at 105.9 ppm in this spectrum can be assigned to either C-10 or C-15 or both. The narrow line-width (FWHM of 49 Hz) indicates that the position might belong to the donor. The signal at 96.9 ppm can be assigned to the C-5 methine carbon most probably of a Chl *a*.

The narrow line-width of most of the signals indicates a monomeric and rigid donor. No hints for polarisation located on the second electron transfer branch can be observed, so it appears that only one of the two possible electron transfer pathways within PS II is active. Most of the polarisation has been observed on the donor site. Since some signals cannot be clearly assigned to the donor or the acceptor (e.g., the signals at 168.4 ppm and 152.1 ppm), it cannot be ruled out completely that there is some polarisation on the primary electron acceptor (Phe *a*). An overview of the resonances enhanced by the solid-state photo-CIDNP effect is given in Table 3.

400 MHz NMR spectrum: A number of 18 light-induced signals appear upon continuous illumination with white light from which two are absorptive and the rest is emissive. The most deshielded signal arises at 192.0 ppm and can be assigned to the C-13^1 of the donor. The strongest signals can be observed in the aromatic region between 133.7 and 168.1 ppm. The latter one could be assigned to both: Chl *a* or Phe *a* cofactor. The rather narrow line-width (FWHM of 54 Hz) indicates that the signal belongs to the donor. The signal at 161.6 ppm (43 Hz) can be assigned to the C-14 of the donor. A rather weak resonance at 160.5 ppm may arise from the C-16 of Phe *a*. The C-1 of the Chl *a* donor is most likely causing the signal at 155.9 ppm with a typically narrow line-shape (FWHM of 40 Hz) of a rigid donor. The emissive

resonance at 153.8 ppm can be assigned to the C-6 of Phe *a*, which is also reflected by the slightly higher line-width of about 70 Hz.

There are only two light-induced resonances observed which are absorptive: the signal at 152.4 ppm and the one resonating at 143.1 ppm. The first one might be induced by a C-16 of Chl *a*, which is also supported by the narrow line-width of about 45 Hz. The second signal at 143.1 ppm can be assigned to the C-1 of the primary electron acceptor which is in good agreement with the literature (Janssen 2013)

The emissive signal at 151.3 ppm can be assigned to the C-14 of Phe *a* which is supported by the broad line-width of 75 Hz. The resonances at 148.4 ppm can be assigned to the Chl *a* C-4, again in good congruence with literature data (Janssen 2013). It cannot be decisively concluded whether C-9 or C-11of Chl *a* is resonating at 147.7 ppm. The narrow line-shape (FWHM of 47 Hz) indicates that the signal is caused by only one of these positions. The strongest resonance can be observed 145.4 ppm and could be induced by the C-8 position of either Chl *a* or Phe *a*. However, the line-width of about 50 Hz indicates, that this signal is only induced be the Chl *a* position.

The emissive resonance at 139.7 ppm, which has a line-width of 80 Hz, might be due to the C-3 position of the primary electron acceptor. A signal at a similar position has also been attributed as an alternative electron spin carrier which might be histidine or another part of the protein matrix (Janssen 2013). The resonance at 135.5 ppm could be assigned to the C-2 of the Chl *a* donor. The signal observed at 133.7 ppm might arise from either the C-7 of Chl *a* or the axial ligating histidine, most probably from the γ-C position. The weak resonance at 117.9 ppm might arise from the δ-carbon of histidine The most shielded light-induced signal resonates at

106.1 ppm most probably due to C-10 or C-15 of either Chl *a* or Phe *a*. The line-width of about 50 Hz again provides a hint that the signal arises from the donor.

Except for the signals assigned to the protein, all signals have been assigned to either a single Chl *a* or a single Phe *a* position. This implies that only one of the two possible electron transfer branches in PS II is active, a conclusion which is consistent with the literature (Janssen 2013).

3.3.2 The origin of the sign-change of many light-induced signals at different magnetic fields

In the photo-CIDNP spectrum A in Fig. 11, obtained at 4.7 T, a number of nine light-induced signals can be observed of which eight are enhanced absorptive and only one is emissive. Spectra obtained from spinach and duckweed at the same field appear very similar to the one presented here (Janssen 2013). Only some of the signals reported in this work appear with weaker intensity. The similarity in the chemical shifts and the intensity patterns of the spectra observed on spinach, duckweed and *P. tricornutum* support the idea (Barber 2006; Green and Durnford 1996) that in eukaryotic species, the pigment-protein complex of PS II is highly conserved.

In contrast to this, in spectrum B of Fig. 11, measured at 9.4 T, 17 of the total 19 light-induced signals are emissive. Photo-CIDNP MAS NMR spectra of PS II in the literature (Diller et al. 2005) are always characterized by a pattern comprised of mostly enhanced absorptive signals. Therefore, the mainly emissive pattern of the PS II core complex preparation of *P. tricornutum* is indeed a surprise.

The data imply that the sign change is most probably due to a decrease of the extent of the DR which is itself caused by a shorter-lived molecular triplet state at higher field which is quenched, if there is a carotenoid nearby. A previous work on PS I core complexes showed that the DR

mechanism is not active or contributes only very slightly to the total nuclear spin polarisation leading to typically emissive signals (Zill et al. 2017b). It was shown that the extent of the effect is increasing with decreasing magnetic field (Thamarath et al. 2012). In the type-II bacterial RC of *R. sphaeroides* the DR has only been observed, if there was a carotenoid in close vicinity to the donor, whereas for the carotenoidless mutant R26 strong DR could be detected (Scheme 1) (Jeschke and Matysik 2003). The life-time of the molecular triplet state correlates to the distance of the quenching molecule, typically a carotenoid, and the donor. In case of the bacterial RC of the *R. sphaeroides* wild-type, the donor-carotenoid distance is 8.6 Å which is reflected by the short triplet life-time of 100 ns. For plant PS I the cofactor arrangement is slightly different, whereby the shortest Chl *a*-carotenoid distance is 10.6 Å and the molecular donor triplet has a half-life of 5 μs (Sétif and Brettel 1990). Since the donor-carotenoid distance is 20.2 Å in plant PS II (Wei et al. 2016) the triplet life-time is long enough to allow the DR to be operative. For the PS II sample from *P. tricornutum* the multitude of emissive signals raises the question, whether the DR is still operating in this sample at 9.4 T. This would imply that even though the protein subunits in eukaryotic PS II complexes are conserved, the cofactor arrangement might be different. The carotenoid seems to have a shorter distance to the donor in the PS II, similar to the situation in the plant PS I but not the plant PS II.

Most recently, another unexpected sign change has been observed in RCs of *Rhodobacter sphaeroides* WT at magnetic fields in the millitesla range in a shuttle-MAS NMR experiment (Gräsing et al. 2017), and presently in our laboratory research is going to understand this phenomenon more adequately.

3.3.3 The involvement of histidine in the solid-state photo-CIDNP effect

In the ^{15}N NMR spectrum shown in Fig. 6, two signals resonating at 224.9 and 243.7 ppm were observed. These signals carry much lower electron spin density as compared to the Chl and Phe cofactors. Previous photo-CIDNP studies on PS II from spinach have shown that the histidine in the surrounding protein matrix ligating to the donor Chl *a* also obtains polarization (Diller et al. 2007a). In that study, a photo-CIDNP MAS NMR signal at 243.8 ppm has been assigned to the π-nitrogen of the histidine residue. Interestingly, in this work a ^{15}N signal at 243.7 ppm was observed from the PS II RC of the diatiom *P. tricornutum*, which can be safely assigned to the π-nitrogen of histidine ligating to the donor Chl *a*. In addition, we detected another signal at 224.9 ppm, which has not been observed in any photo-CIDNP spectrum from PS II. The signal at 224.9 ppm matches very well with the assignment of τ-nitrogen of the histidine which ligates to the Mg^{2+} of the Chl. This assignment is based on the ^{15}N resonances of the imidazole side chain of histidine in LHC II (Alia et al. 2001) and in bacterial RCs of *R. sphaeroides* (Alia et al. 2009) detected with MAS NMR. Since the two accessory chlorophylls in PS II, Chl_{D1} and Chl_{D2}, are not coordinated to histidine, this implies that P_{D1} or P_{D2} and the histidine ligating to the donor Chl get polarized. For comparison, a view on the histidine-198 ligating to Mg^{2+} of Chl *a* in the x-ray structure of PS II from spinach is presented in Fig. 13 (Wei et al. 2013). This complex of histidine and Chl *a* appears as the electron donor in PS II from *P. tricornutum*. Based on the ^{15}N chemical shift value of histidine, we can conclude that this histidine is most likely neutral in character and carrying an electron lone pair at the π-position (243.7 ppm) while the τ-nitrogen is ligated to Mg^{2+} of the Chl (224.9 ppm).

To gain further insight into the electronic structure and charge states of axial histidines, we analysed the ^{13}C photo-CIDNP MAS NMR spectrum obtained from the PS II core complexes of the diatom *P. tricornutum*.

Interestingly, the ^{13}C photo-CIDNP MAS NMR spectra also show a set of three clear signals which all can be attributed to a histidine (Fig. 11 and Table 3). These signals appear at 117.9, 133.7 and 136.8 ppm and were assigned to the δ-, γ- and ε-carbon of the imidazole ring of histidine based on the previous ^{13}C assignment of histidine in LHC II and bacterial RC which were obtained by using solid-state MAS NMR (for comparison see Table 4) (Alia et al. 2001; Alia et al. 2009). Based on the ^{13}C resonances of the δ- and the γ-carbon, it can be further confirmed that the histidine seen in the photo-CIDNP MAS NMR spectra of the PS II of the diatom *P. tricornutum* is most likely neutral in character (Scheme 2).

4 Conclusions

It is demonstrated that the solid-state photo-CIDNP effect can be observed in the Bacillariophyceae class of the diatom phylum. We have shown the effect in four experiments: (I) on a ^{15}N labelled sample from *P. tricornutum* containing both PSI and PSII and (II) with ^{13}C photo-CIDNP MAS NMR on the same sample as well as on a PS II core complex preparation from the same species at 4.7 T (III) and at 9.4 T (IV). Therefore, it appears to be plausible that the effect can be observed in all phototrophic species, since it was found in nine different species from all three phototrophic kingdoms and a variety of phyla, so far. Hence, the effect seems to be conserved in all phototrophic species. It appears that the structural features enabling a species to perform photosynthesis are related to the occurrence of the solid-state photo-CIDNP effect.

The signals assigned to PS I show that most electron spin density is located on only one branch of intrinsic PS I electron transport. However, a minor part of the electron spin density seems to be localized on the other branch. It appears that the ^{15}N photo-CIDNP MAS NMR pattern of PS I from *P. tricornutum* is more similar to the PS I pattern of duckweed than to that of spinach.

In PS I most of the electron spin density is observed on the donor and the primary electron acceptor of one branch. Only a small quantity might be assigned to the other branch. All signals can be assigned to Chl *a* cofactors in PS I.

In the case of PS II, most signals have been assigned to the Chl *a* and Phe *a* cofactors of only one branch, as found in higher plants. In addition to the resonances from Chl *a* and Phe *a*, some signals originating from PS II can be assigned to a specific histidine residue. For the first time, a complete set of all five positions of the imidazole ring are assigned in the ^{13}C and ^{15}N solid-state MAS NMR spectra. Hence, the electron donor in PS II from *P. tricornutum* must be Chl *a*-histidine-complex. It appears that in the Chl-histidine complex, the histidine provides partial charge to the Chl. The ^{15}N photo-CIDNP pattern of PS II from *P. tricornutum* is very similar to the one observed from spinach (Diller et al. 2007b). Based on proteomic and genomic data, it is expected that both PSs are highly conserved in plants as well as in the diatom phylum (Barber 2006; Green and Durnford 1996; Lepetit 2010). The presented data strongly suggest, that the inversion of the photo-CIDNP signals at 9.4 T with respect to the spectrum at 4.7 T is caused by a decrease of the DR mechanism. This leads to the assumption that a carotenoid cofactor might be closer in PS II of *P. tricornutum* compared to PS II preparations from higher plants. Since no x-ray structures of diatom PSs exist, the present study provides the first evidence that the cofactor arrangement in the diatom PS II RC is different compared to that in higher plants.

The photo-CIDNP MAS NMR spectra of both samples show narrow peaks assigned to the donor, which indicates a very rigid structure of the electron donor. This is common in all photosynthetic RCs. Although no x-ray data of photosystems of diatoms are available, photo-CIDNP MAS NMR has been able to perform a detailed analysis of the properties of the photochemical machinery.

Acknowledements: The authors want to thank Dr. Matthias Findeisen for technical support.

Compliance with Ethical Standards: Funding: This study was funded by the Deutsche Forschungsgemeinschaft DFG (MA4972/2-1). Conflict of Interest: All authors declares that they have no conflict of interest.

References

Alia A, Matysik J, Soede-Huijbregts C, et al. (2001) Ultrahigh Field MAS NMR Dipolar Correlation Spectroscopy of the Histidine Residues in Light-Harvesting Complex II from Photosynthetic Bacteria Reveals Partial Internal Charge Transfer in the B850/His Complex. J. Am. Chem. Soc. 123, 4803-4809. doi: 10.1021/ja002591z

Alia A, Roy E, Gast P et al (2004) Photochemically induced dynamic nuclear polarization in photosystem I of plants observed by ^{13}C magic-angle spinning NMR. J. Am. Chem. Soc. 126, 12819-12826. doi:10.1021/ja048051+

Alia A, Wawrzyniak PK, Janssen GJ, et al. (2009) Differential Charge Polarization of Axial Histidines in Bacterial Reaction Centers Balances the Asymmetry of the Special Pair. *J. Am. Chem. Soc. 131*, 9626-9627. doi: 10.1021/ja9028507

Allen AE, Dupont CL, Oborník M, Horák A, Nunes-Nesi A, Mc Crow JP, Zheng H, Johnson DA, Hu H, Fernie AR, Bowler C (2011) Evolution and metabolic significance of the urea cycle in photosynthetic diatoms. *Nature 473*, 203-207. doi: 10.1038/nature10074

Allen JP, Williams JC (1998) Photosynthetic reaction centers. FEBS Letters 438, 5-9. DOI: 10.1016/S0014-5793(98)01245-9.

Amunts A, Drory O, Nelson N (2007) The structure of a plant photosystem I supercomplex at 3.4 Å resolution. Nature 447, 58-63. doi: 10.1038/nature05687

Amunts A, Nelson N (2008) Functional organization of a plant Photosystem I: evolution of a highly efficient photochemical machine. Plant Physiol. and Biochem. 46, 228-237. doi: 10/1016.j.plaphy.2007.12.013

Armbrust EV, Berges JA, Bowler C, et al. (2004) The genome of the diatom thalassiosira pseudonana: ecology, evolution, and metabolism. *Science 306*, 79-86. doi: 10.1126/science.1101156

Armbrust EV (2009) The life of diatoms in the world´s oceans. *Nature 459*, 185-19. doi 10.1038/nature08057

Barber J (2006) Photosystem II: an enzyme of global significance. *B*iochem. Soc. Trans. 34, 619-631. doi: 10.1042/BST0340619

Bennett AE, Rienstra CM, Auger M, Lakshmi KV, Griffin RG (1995) Heteronuclear decoupling in rotating solids. J. Chem. Phys. 103, 6951-6958. doi: 10.1063/1.470372.

Ben-Shem A, Frolow F, Nelson N (2003) Crystal structure of plant photosystem I. *Nature 426*, 630-635. doi: 10.1038/nature02200

Benson DA, Karsch-Mizrachi I, Lipman DJ, Ostell J, Sayers EW (2009), Nucleic Acids Res. 37 (Database issue): D26-31, Epub 2008 Oct 21. doi: 10.1093/nar/gkn723

Bielecki A, Burum DB (1995) Temperature-dependence of ^{207}PB MAS spectra of solid lead nitrate: An accurate, sensitive thermometer for variable-temperature MAS. J. Magn. Reson. 116, 215-220.

Bode B, Thamarath SS, Sai Sankar Gupta KB, Alia A, Jeschke G, Matysik J (2013) The solid-state photo-CIDNP effect and its analytical application. In: Hyperpolarization methods in NMR spectroscopy (Kuhn L ed.) Springer, pp. 105-121.

Boender GJ (1996) Ph.D. Thesis, Dissertation, Univ. Leiden.

Bowler C, Allen AE, Badger JH, et al. (2008) The Phaeodactylum genome reveals the evolutionary history of diatom genomes. *Nature 456*, 239-244.

Boxer SG, Closs GL, Katz JJ (1974) The effect of magnesium coordination on the ^{13}C and ^{15}N magnetic resonance spectra of chlorophyll *a*. Energies of nitrogen n_{π}^* states as deduced from a the relative complete assignment of chemical shifts. *J. Am. Chem. Soc. 9*6, 7058-7066. doi:10.1021/ja00829a038

Bryant DA, Garcia Costas AM, Maresca JA et al. (2007) *Candidatus* Chloracidobacterium thermophilum: an aerobic phototrophic acidobacterium. *Science 317*, 523-526. doi:10.1126/science.1143236Cavalier-Smith T (1998) A revised six-kingdom system of life. Biol. Rev. 73, 203-266.

Céspedes-Camacho IF, Matysik J (2014) Spin in Photosynthetic Electron Transport. In: "The Biophysics of Photosynthesis" (J. Golbeck & Art van der Est, Eds.), Springer, New York, pp. 141-170.

Daviso E, Jeschke G, Matysik J (2008) Photochemically induced dynamic nuclear polarization (Photo-CIDNP) magic-angle spinning NMR. Biophysical Techniques in Photosynthesis (Aartsma TJ, Matysik J, eds.), Springer, Dordrecht, pp. 385-399.

Daviso E, Prakash S, Alia A et al. (2009) The electronic structure of the primary electron donor of reaction centers of purple bacteria at the atomic resolution as observed by photo-CIDNP 13C MAS NMR. Proc. Natl. Acad. Sci. USA 106, 22281-22286.

Dekker JP, Boekema EJ (2005) Supramolecular organization of thylakoid membrane proteins in green plants. *Biochim*. Biophys *Acta 1706*, 12-39. doi: 10.1016/j.bbabio.2004.09.009

Deligiannakis Y, Rutherford A (2001) Electron spin echo envelope modulation spectroscopy in photosystem I. *Biochim. Biophys. Acta 1507*, 226- 246. doi: 10.1016/S0005-2728(01)00201-8

Diller A, Alia A, Roy E et al (2005) Photo-CIDNP solid-state NMR on photosystems I and II: what makes P680 special? *Photosynth. Res. 84*, 303-308. doi:10.1007/s11120-005-0411-0

Diller A, Roy E, Gast P et al. (2007a) ^{15}N photochemically induced dynamic nuclear polarization magic-angle spinning NMR analysis of the electron donor of photosystem II. *Proc. Natl. Acad. Sci. USA 104*, 12767-12771. doi:10.1073/pnas.0701763104

Diller A, Prakash S, Alia A, Gast P, Matysik J, Jeschke G (2007b) Signals in solid-state photochemically induced dynamic nuclear polarization recover faster than with the longitudinal relaxation time *J. Phys. Chem. B* 111, 10606-10614. doi: 10.1021/jp072428r

Diller A, Alia A, Gast P et al (2008) ^{13}C Photo-CIDNP MAS NMR on the LH1-RC Complex of *Rhodopseudomonas acidophilia*. In: Energy from the sun. (Allen JF, Gantt E, Golbeck JH, Osmond B, eds.) Dordrecht, Springer, pp 55-58.

Dyballa N, Metzger S (2009) Fast and sensitive colloidal coomassie G-250 staining for proteins in polyacrylamide gels. *J. Vis. Exp. 30*, 1431. : doi: 10.3791/1431

Egorova-Zachernyuk TA, van Rossum B, Boender GJ, et al. (1997) Characterization of Pheophytin Ground States in Rhodobacter sphaeroides R26 Photosynthetic Reaction Centers from Multispin Pheophytin Enrichment and 2-D 13C MAS NMR Dipolar Correlation Spectroscopy. Biochemistry 36, 7513-7519. doi: 10.1021/bi962770m

Ferreira KN, Iverson TM, Maghlaoui K, Barber J, Iwata S (2004) Architecture of the photosynthetic oxygen-evolving center. *Science 303*, 1831-1838. doi: 10.1126/science.1093087

Fischer MR, de Groot HJM, Raap J, Winkel C, Hoff AJ, Lugtenburg J (1992) Carbon-13 magic angle spinning NMR study of the light-induced and temperature-dependent changes in

Rhodobacter sphaeroides R26 reaction centers enriched in [4'-13C]tyrosine. *Biochemistry 31*, 11038-11049. doi: 10/1021/bi00160a013

Flori S, Journeau P-H, Bailleul B et al. (2017) Plastid thylakoid architecture optimizes photosynthesis in diatoms, Nature Communication 8, 15885, doi: 10.1038/ncomms15885

Gibbs SP (1962) The ultrastructure of the chloroplasts of algae, *Ultrastructure Research 7*, 418-435. doi: 10.1016/S0022-5320(62)90038-2

Gibbs SP (1970) The comparative ultrastructure of the algal chloroplast. *Ann. New York Acad. Sci. 175*, 454-473. doi: 10.1111/j.1749-6632.1970.tb45167.x

Goessling JW, Su YCartaxana P, et al. (2018) Structure-based optics of centric diatom frustules: modulation of the in vivo light field for efficient diatom photosynthesis. *New Phytologist 219*, 122-134 doi: 10.1111/nph.15149

Goss R, Lepetit B (2015) Biodiversity of NPQ. *J Plant Physiol. 172*, 13-32. doi: 10.1016/j.jplph.2014.03.004

Gräsing D, Bielytskyi P, Céspedes-Camacho IF, Alia A, Marquardsen T, Engelke F, Matysik J (2017) Field-cycling NMR with high-resolution detection under magic-angle spinning: determination of field-window for nuclear hyperpolarization in a photosynthetic reaction center. *Scientific Reports, 7,* 12111. DOI:10.1038/s41598-017-10413-y.

Green BR, Durnford DG (1996) The chlorophyll-carotenoid proteins of oxygenetic photosynthesis. *An. Rev. Plant Physiol. Plant Mol. Biol. 47*, 685-714. doi: 10.1146/annurev.arplant.47.1.685

Grouneva I, Jakob T, Wilhelm C, Goss R. (2009) The regulation of xanthophyll cycle activity and of non-photochemical fluorescence quenching by two alternative electron flows in the

diatoms Phaeodactylum tricornutum and Cyclotella meneghiniana. Biochim Biophys Acta. 1787, 929-938.

Guskov A, Kern J, Gabdulkhakov A, Broser M, Zouni A, Saenger W (2009) Cyanobacterial photosystem II at 2.9-angstrom resolution and the role of quinones, lipids, channels and chloride. Nature Structural & Molecular Biology 16, 334-342. doi: 10.1038/nsmb.1559

Haynes WM (Ed.) (2015) CRC Handbook of Chemistry and Physics, CRC Press, Boca Raton, pp. 3-142.

Li S, Hong M (2011) Protonation, Tautomerization, and Rotameric Structure of Histidine: A Comprehensive Study by Magic-Angle-Spinning Solid-State NMR. J. Am. Chem. Soc. 133, 1534-1544. doi: 10.1021/ja108943n.

Janssen GJ, Daviso E, van Son M et al. (2010) Observation of the solid-state photo-CIDNP effect in entire cells of cyanobacteria *Synechocystis*. *Photosynth. Res. 104*, 275-282. doi:10.1007/s11120-009-9508-1.

Janssen GJ, Roy E, Matysik J, Alia A (2012) ^{15}N photo-CIDNP MAS NMR to reveal functional heterogeneity in electron donor of different plant organisms. *Appl. Magn. Reson. 42*, 57-67. doi:10.1007/s00723-011-0283-8

Janssen GJ (2013) The Heart of Oxygenetic Photosynthesis illuminated, Dissertation, Univ. Leiden.

Jensen PE, Bassi R, Boekema EJ, et al. (2007) Structure, function and regulation of plant photosystem I. *Biochim. Biophys. Acta 1767*, 335-352. doi: 10.1016/j.bbabio.2007.03.004

Jeschke G (1998) A new mechanism for chemically induced dynamic nuclear polarization in the solid state. *J. Am. Chem. Soc. 120*, 4425-4429. doi:10.1021/ja973744u.

Jeschke G, Matysik J (2003) A reassessment of the origin of photochemically induced dynamic nuclear polarization effects in solids. *Chem. Phys. 294*, 239-255. doi:10.1016/S0301-0104(03)00278-7.

Jordan P, Fromme P, Witt HAT et al. (2001) Three-dimensional structure of cyanobacterial photosystem I at 2.5 Å resolution. *Nature 411*, 909-917. doi: 10.1038/35082000.

Käß H, Lubitz W (1996) Evaluation of 2D-ESEEM data of 15N-labeled radical cations of the primary donor P700 in photosystem I and chlorophyll a. Phys. Lett. 251, 193-203.

Kustka AB, Allen AE, Morel FMM (2007) Sequence analysis and transcriptional regulation of iron acquisition genes in two marine diatoms. *J. Phycol. 43*, 715-729. doi: 10.1111/j.1529-8817.2007.00359.x

Laemmli UK (1970) Cleavage of Structural Proteins during the Assembly of the Head of Bacteriophage T4. *Nature 227*, 680-685. doi: 10.1038/227680a0.

Lavaud J, Goss R (2014) Non-Photochemical Quenching and Thermal Energy Dissipation In Plants, Algae and Cyanobacteria, Series: Advances in Photosynthesis and Respiration, In: Demmig-Adams B, Adams III WW, Garab G, Govindjee (Eds.), Springer-Dordrecht.

Lavaud J, van Gorkom HJ, Etienne A (2002), Photosystem II electron transfer cycle and chlororespiration in planktonic diatoms. *Photosynth. Res. 74*, 51-59. doi: 10.1023/A:1020890625141.

Lepetit B, Volke D, Szabó M, Hoffmann R, Garab G, Wilhelm C, Goss R (2007) Spectroscopic and molecular characterization of the oligomeric antenna of the diatom Phaeodactylum tricornutum. *Biochemistry 46*, 9813-9822. doi: 10.1021/bi7008344

Lepetit B (2010) Untersuchungen zur Struktur der Antennenkomplexe und zur Lokalisation der Xanthophyllzykluspigmente in Diatomeen, Dissertation, Universität Leipzig.

Loll B, Saenger W, Zouni A, Biesiadka J (2005) Towards complete cofactor arrangement in the 3.0 Å resolution structure of photosystem II. *Nature 438*, 1040-1044. doi: 10.1038/nature04224.

Lommer M. Specht M, Roy A-S, et al. (2012) Genome and low-iron response of an oceanic diatom adapted to chronic iron limitation. *Genome Biology 13*, 1-20. doi: 10.1186/gb-2012-13-7-r66

Mac M, Tang X-S, Diner BA, McCracken J, Babcock GT (1996) Identification of histidine as an axial ligand to P700+. *Biochemistry 35*, 13288-13293. doi: 10.1021/bi961765f

Mann DG, Droop SJM (1996) Biodiversity, biogeography and conservation of diatoms. *Hydrobiologia 336*, 19-32. doi: 10.1007/BF00010816

Matysik J, Alia A, Hollander JG et al. (2000) A set-up to study photochemically induced dynamic nuclear polarization in photosynthetic reaction centres by solid-state NMR. *Indian J. Biochem. Biophys. 37*, 418.

Matysik J, Diller A, Roy E, Alia A (2009) The solid-state photo-CIDNP effect. *Photosynth Res 102*, 427-435. doi: 10.1007/s11120-009-9403-9

McDermott A, Zysmilich MG, Polenova T (1998) Solid state NMR studies of photoinduced polarization in photosynthetic reaction centers: mechanism and simulations. *Solid State Nucl. Magn. Reson. 11*, 21-47. doi:10.1016/S0926-2040(97)00094-5.

Mock T, Otillar RP, Strauss J et al. (2017) Evolutionary genomics of the cold-adapted diatom Fragilariopsis cylindrus. *Nature 541*, 536-540. doi: 10.1038/nature20803

Nagao R, Tomo T, Noguchi E, et al. (2009) Purification and characterization of a stable oxygen-evolving Photosystem II complex from a marine centric diatom, Chaetoceros gracilis. Biochim. Biophys. Acta, **2010**, 1797, 160-166. doi: 10.1016/j.bbabio.2009.09.008

Nagao R, Suga M, Niikura A et al. (2013) Crystal structure of Psb31, a novel extrinsic protein of PSII from a marine centric diatom and implications for ist binding and function. Biochemistry 52, 6646-6652. doi: 10.1021/bi400770d

Najdanova M, Janssen GJ, de Groot HJM et al. (2015) Analysis of electron donors in photosystems in oxygenic photosynthesis by photo-CIDNP MAS NMR. J. Photochem. Photobiol. B 152, 261-271. doi 10.1016/j.jphotobiol.2015.08.001

Polenova T, McDermott AE (1999) A coherent mixing mechanism explains the photoinduced nuclear polarization in photosynthetic reaction centers. *J. Phys. Chem. 103*, 535-548. doi:10.1021/jp9822642

Prakash S, Alia A, Gast P, de Groot HJM, Jeschke G, Matysik J (2005a) Magnetic field dependence of photo-CIDNP MAS NMR on photosynthetic reaction centres of *Rhodobacter sphaeroides* WT. *J. Am. Chem. Soc. 127*, 14290-14298. DOI: 10.1021/ja0623616

Prakash S, Tong SH, Alia A, Gast P, de Groot HJM, Jeschke G, Matysik J (2005b) 15N photo-CIDNP MAS NMR on reaction centers of Rhodobacter sphaeroides In Photosynthesis: Fundamental Aspects to Global Perspektives, Allen Press, Montreal, pp. 236-238.

Prakash S, Alia A, Gast P et al. (2006) Photo-CIDNP MAS NMR in intact cells of *Rhodobacter sphaeroides* R26: Molecular and atomic resolution at nanomolar concentration. *J. Am. Chem. Soc. 128*, 12794-12799. doi:10.1021/ja0623616

Pyszniak AM, Gibbs SP (1992) Immunocytochemical localization of photosystem I and the fucoxanthin-chlorophyll*a/c* light-harvesting complex in the diatom*Phaeodactylum tricornutum*. *Protoplasma 166*, 208-218. doi: 10.1007/BF01322783

Roy E, Diller A, Alia A et al. (2007a) Magnetic field dependence of ^{13}C photo-CIDNP MAS NMR in plant photosystems I and II. *Appl. Magn. Reson. 31*,193-204. doi:10.1007/BF03166256.

Roy E, Alia A, Gast P et al. (2007b) Photochemically induced dynamic nuclear polarization in the reaction center of the green sulphur bacterium *Chlorobium tepidum* observed by ^{13}C MAS NMR. *Biochim Biophys Acta 1767*, 610-615. doi:10.1016/j.bbabio.2006.12.012

Roy E, Rohmer T, Gast P et al. (2008) Characterization of the primary radical pair in reaction centers of *Heliobacillus mobilis* by ^{13}C Photo-CIDNP MAS NMR. *Biochemistry 47*, 4629-4635. doi:10.1021/bi800030g.

Sayers EW, Barrett T, Benson DA et al. (2009) Database resources of the National Center for Biotechnology Information. *Nucleic Acids Res.*, **2009**, *37*, Epub 2008 Oct 21. doi: 10.1093/nar/gkn741

Schubert WD, Klukas O, Saenger W et al. (1998) A common ancestor for oxygenetic and anoxygenetic photosynthetic systems: a comparison based on the structural model of photosystem I. *J. Mol. Biol. 280*, 297-314. doi: 10.1006/jmbi.1998.1824SDBS: Spectral Database for Organic Compounds (1999) National Institute of Advanced Industrial Science and Technology, NMR: K. Haya- mizu, M. Yanagisawa, O. Yamamoto, MS: N. Wasada, ESR: K. Someno, IR: K. Tanabe, T. Tamura, Raman: K. Tanabe, J. Hiraishi, ^{13}C NMR spectrum; SDBS No.: 1188 CDS-07-029, http://sdbs.db.aist.go.jp/sdbs/cgi-bin/direct_frame_top.cgi (Accessed January 20, 2017).

Sétif P, Brettel K (1990) Photosystem I photochemistry under highly reducing conditions: Study of the P700 triplet state formation from the secondary radical pair (P700+−A−1). *Biochim. Biophys. Acta 1020*, 232-238. doi: 10.1016/0005-2728(90)90152-T

Shuvalov VA, Parson WW (1981) Energies and kinetics of radical pairs involving bacteriochlorophyll and bacteriopheophytin in bacterial reaction centers. *Proc. Natl. Acad. Sci. USA*, *78*, 957-961.

Smetacek V (1999) Diatoms and the ocean carbon cycle. *Protist. 150*, 25-32. doi: 10.1016/S1434-4610(99)70006-4

Smetacek V (2000) Oceanography: The giant diatom dump. *Nature 406*, 574-575. doi: 10.1038/35020665.

Sosnovsky D, Jeschke G, Matysik J et al. (2016) Level crossing analysis of chemically induced dynamic nuclear polarization: towards a common description of liquid-state and solid-state cases. *J. Chem. Phys. 144*, 144202. doi: 10.1063/1.4945341.

Sumper M, Brunner E (2008) Silica Biomineralisation in Diatoms: The Model Organism Thalassiosira pseudonana, *ChemBioChem 9*, 1187-1194. doi: 10.1002/cbic.2007007764.

Strzepek RF, Harrison PJ (2004) Photosynthetic architecture differs in coastal and oceanic diatoms. *Nature 431*, 689-692. doi: 10.1038/nature02954.

Thamarath SS, Heberle J, Hore P et al. (2010) Solid-state photo-CIDNP effect observed in phototropin LOV1-C57S by ^{13}C magic-angle spinning NMR spectroscopy. *J. Am. Chem. Soc. 132*, 15542-15543. doi:10.1021/ja1082969

Thamarath SS, Bode BE, Prakash S (2012) Electron spin density distribution in the special pair triplet of Rhodobacter sphaeroides R26 revealed by magnetic field dependence of the solid-state photo-CIDNP effect. J. Am. Chem. Soc., 134, 5921-5930. doi: 10.1021/ja2117377

Tréguer P, Nelson DM, van Bennekom AJ et al. (1995) The silica balance in the world ocean: a reestimate. *Science 268*, 375-379. Doi: 10.1126/science.268.5209.375

Wagner H, Jakob T, Lavaud J, Wilhelm C (2016) Photosystem II cycle activity and alternative electron transport in the diatom Phaeodactylum tricornutum under dynamic light conditions and nitrogen limitation. *Photosynth Res 128*, 151-161. doi: 10.1007/s11120-015-0209-7

Werner D (Ed.) (1977) The Biology of the diatoms, Blackwell Scientific Publikations, Oxford, p. 2

Wilhelm C, Büchel C, Fisahn J, Goss R, Jakob T, LaRoche J, Lavaud J, Lohr M, Riebesell U, Stehfest K, Valentin K, Kroth PG, (2006) The regulation of carbon and nutrient assimilation in diatoms is significantly different from green algae. *Protist*, *157*, 91-124. doi: 10.1016/j.protis.2006.02.003

Wei XP, Zhang XZ, Su XD, et al. (2016) Structure of spinach photosystem II–LHCII supercomplex at 3.2 Å resolution. *Nature 534*, 69-74. doi: 10.1038/nature18020

Wisser D, Brückner SI, Wisser FM, Althoff-Ospelt G, Kaskel S, Brunner E (2015) (1)H-(13)C-(29)Si triple resonance and REDOR solid-state NMR-A tool to study interactions between biosilica and organic molecules in diatom cell walls. *Solid State Nucl. Magn. Reson. 66/67*, 33-39. doi: 10.1016/j.ssnmr.2014.12.007

Zill JC (2017a), Der Festkörper photo-CIDNP-Effekt im Baum des Lebens, Dissertation, Universität Leipzig.

Zill JC, Kansy M, Goss R et al. (2017b) Photo-CIDNP in the reaction center of the datom *Cyclotella meneghiniana* observed by ^{13}C MAS NMR. *Z. Phys. Chem. 231*, 347-367. doi:10.1515/zpch-2016-0806

Zysmilich MG, McDermott A (1994) Photochemically induced dynamic nuclear polarization in the solid-state ^{15}N spectra of reaction centers from photosynthetic bacteria *Rhodobacter sphaeroides* R-26. *J Am Chem Soc 116*, 8362-8363. doi:10.1021/ja00097a052

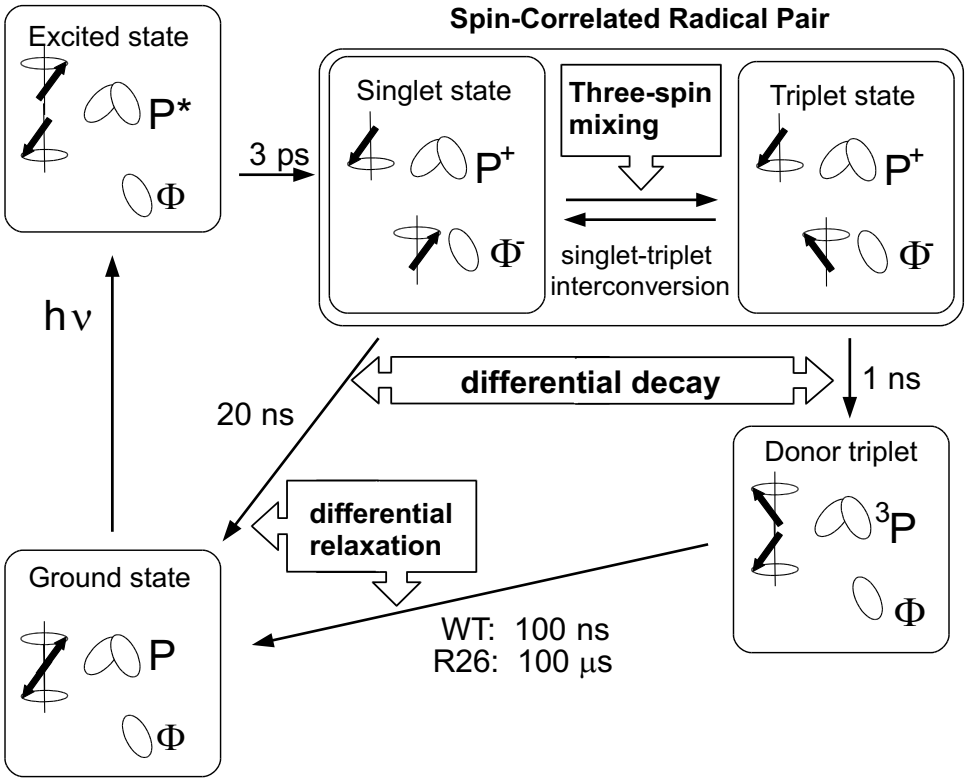

Scheme 1: Photocycle in quinone-blocked bacterial RCs of *Rhodobacter sphaeroides* (Jeschke and Matysik 2003).

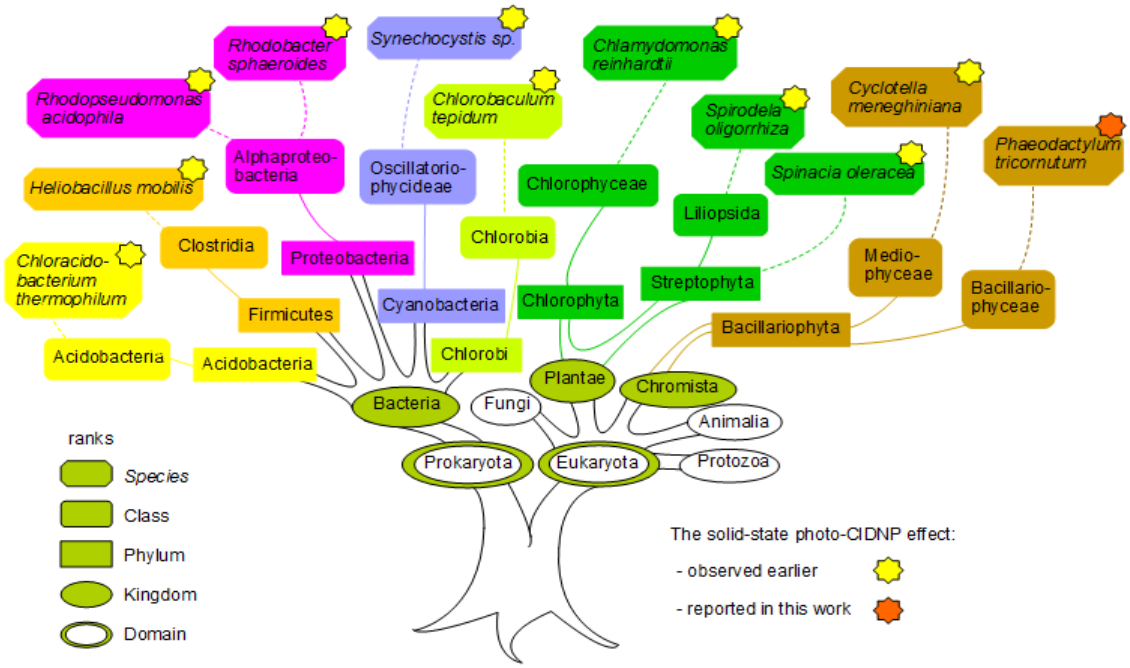

Figure 1: Taxonomic overview according to Cavalier-Smith (Cavalier-Smith 1998), with modifications. Domains and kingdoms containing phototrophic species are labeled in green. So far, the solid-state photo-CIDNP effect has been observed on ten species.(Alia et al. 2004; Bryant et al. 2007; Diller et al. 2005; Diller et al. 2008; Janssen et al. 2010; Janssen et al. 2012; Roy et al. 2007a; Roy et al. 2007b; Roy et al. 2008; Thamarath et al. 2010; Zill 2017a; Zysmilich and MCDermott 1994) The first time observation of the solid-state photo-CIDNP effect in the bacillariophyceae class is reported in this work (orange star).

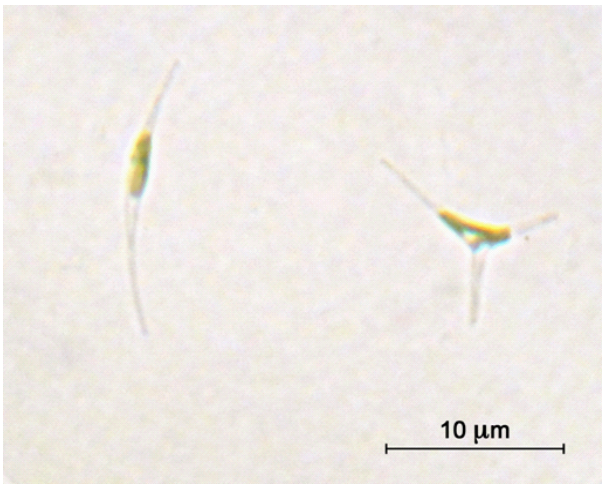

Figure 2: *Phaeodactylum tricornutum*: fusiform (left) and tri-radiate form (right).

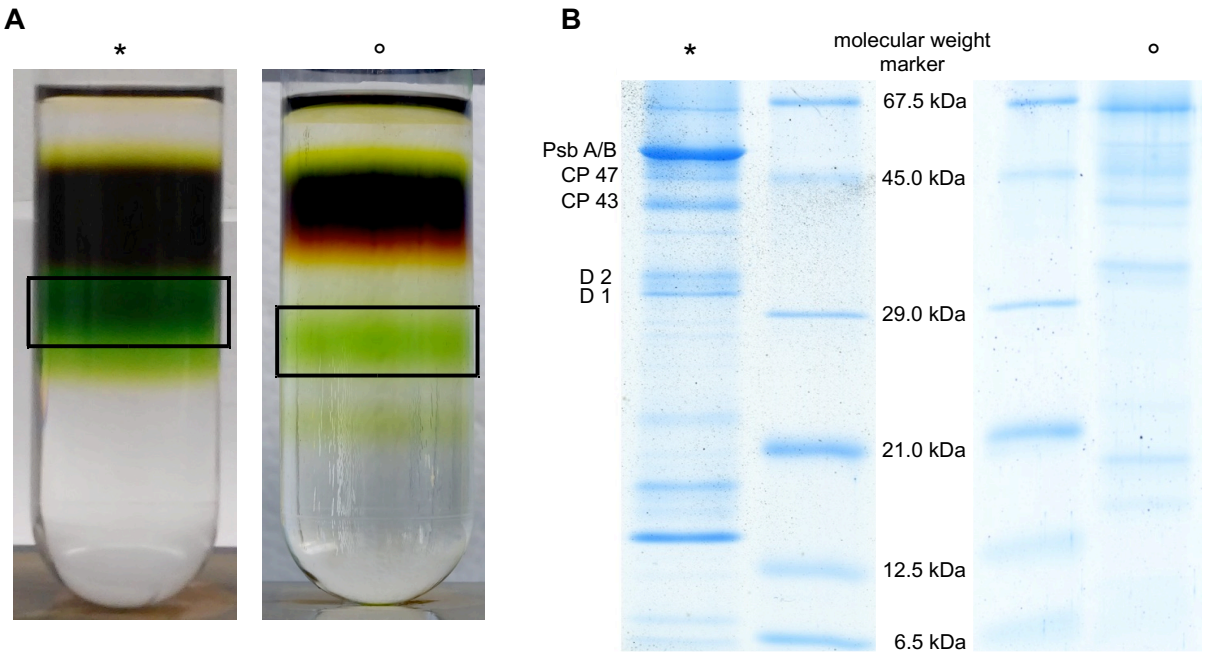

Figure 3: Density gradient used to isolate a PS (PSI and PSII) fraction (A*) and PS II core complexes from *P. tricornutum* (A°). Protein composition determined by SDS-PAGE indicates the presence of both photosystems in the PS fraction which is in-line with results provided by

Nagao et al. 2013, demonstrating a similar molecular weight of monomeric PS II and PS I (B*). The protein composition of the PS II core complex preparation demonstrates a strong enrichment of PS II (B°).

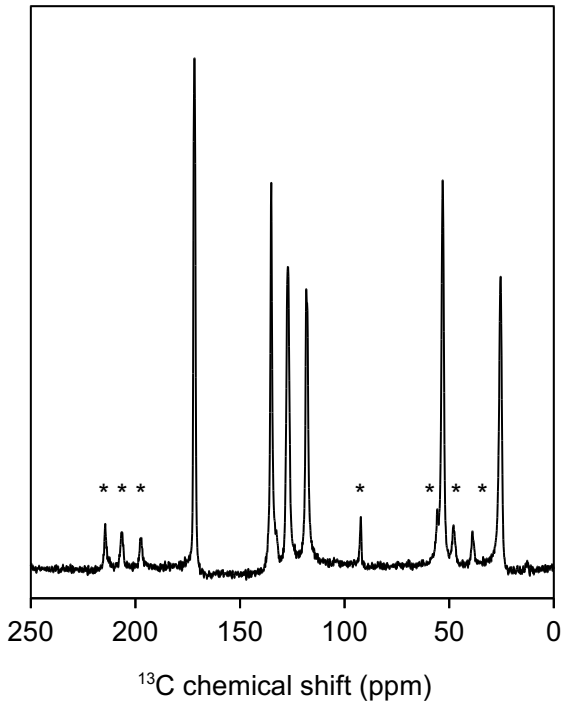

Figure 4: MAS NMR spectrum of solid cationic histidine illustrating the phasing of the external standard. The spectrum was obtained at a magnetic field of 9.4 T and a MAS rotational frequency of 8 kHz. The asterisk (*) refers to spinning sidebands.

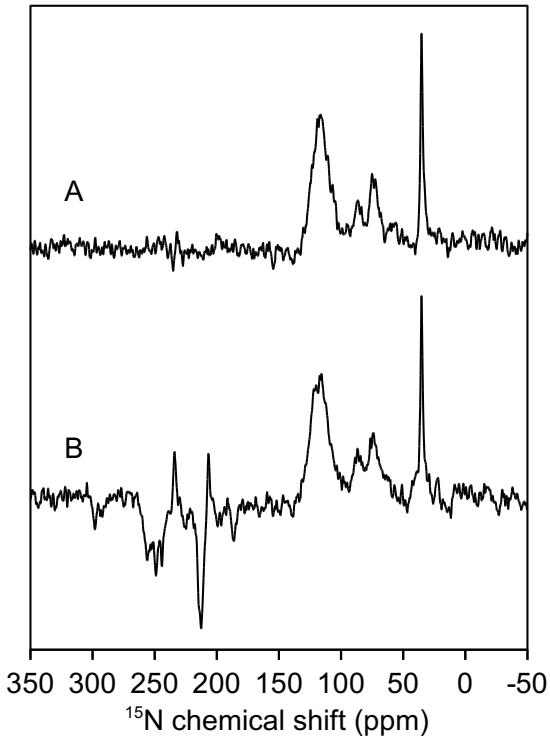

Figure 5: ^{15}N-MAS NMR spectra of the combined PSI and PSII fraction from *P. tricornutum* at 9.4 T. Spectrum A has been recorded in the dark, while spectrum B was obtained under continuous illumination with white light.

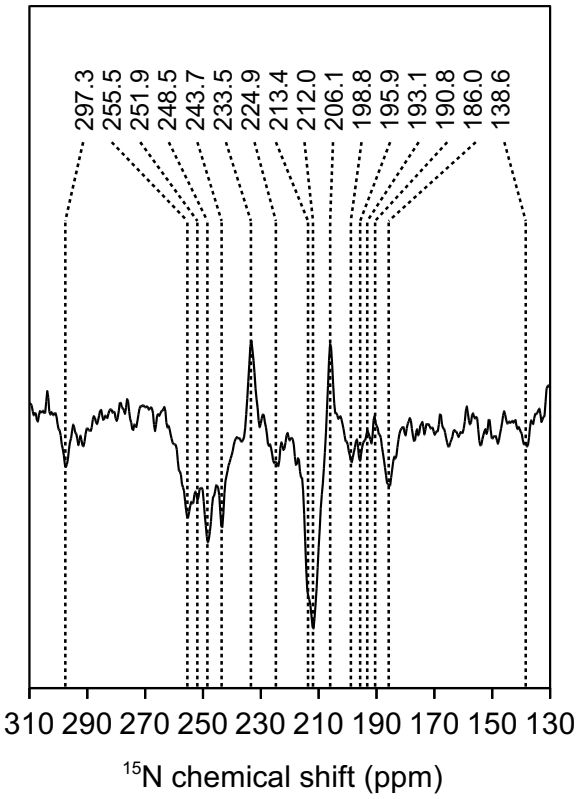

Figure 6: Zoom into the region of light-induced signals in the ^{15}N photo-CIDNP MAS NMR spectrum of the combined PSI and PSII fraction from *P. tricornutum* obtained under continuous illumination (Spectrum 5B).

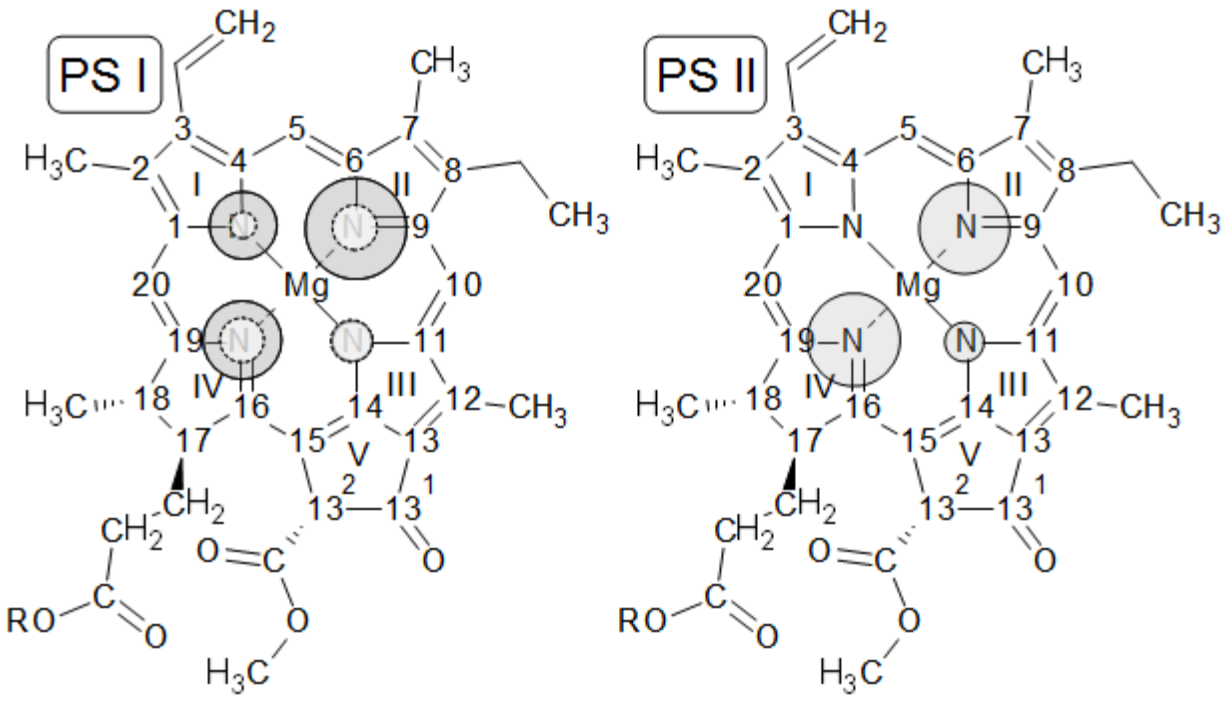

Figure 7: Photo-CIDNP patterns of Chl *a* molecules. left: PS I, Chl *a* acting as donor (solid line) or primary electron acceptor (dashed line). right: PS II, donor Chl *a*. The sizes of the circles are derived from the NMR intensities. R = Phytyl side chain.

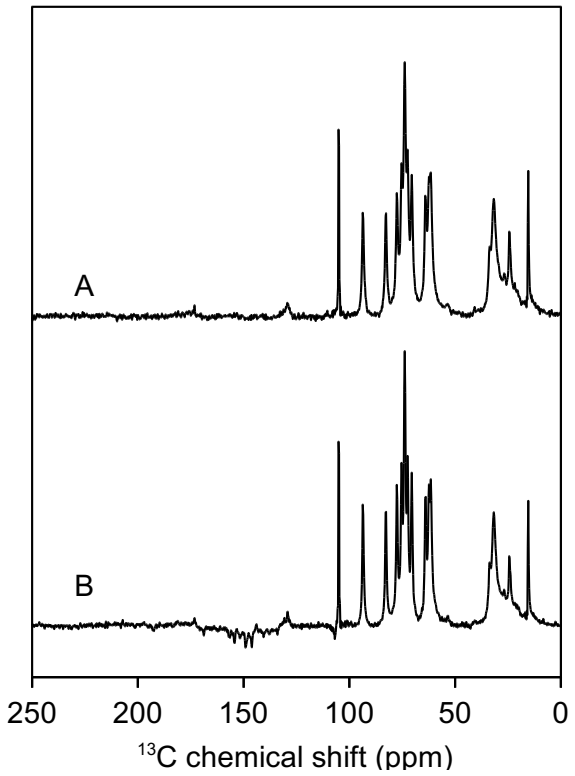

Figure 8: ^{13}C photo-CIDNP MAS NMR of both PSs from *P. tricornutum* at 9.4 T. A: dark spectrum, B: under continuous illumination with white light.

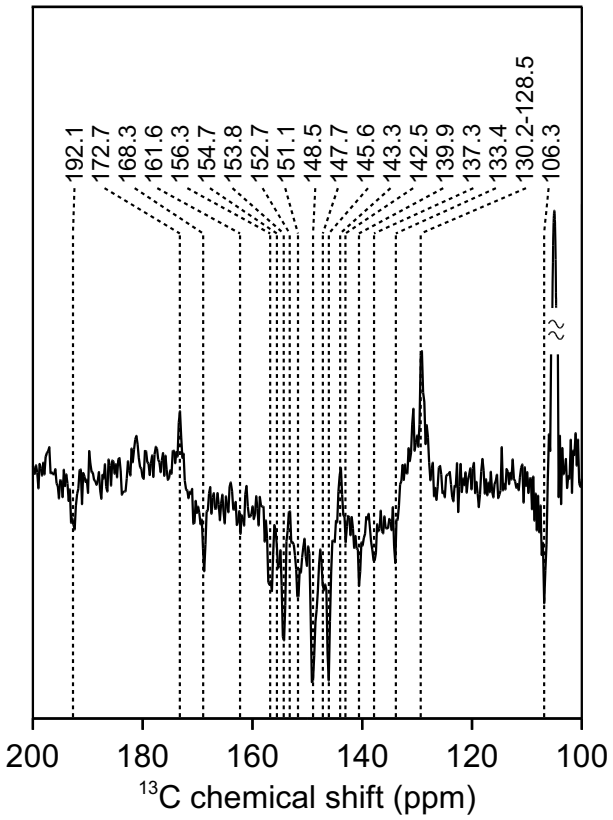

Figure 9: Detailed view on the light-induced signals of the ^{13}C photo-CIDNP MAS NMR spectrum the combined PSI and PSII fraction of *P. tricornutum* under continuous illumination.

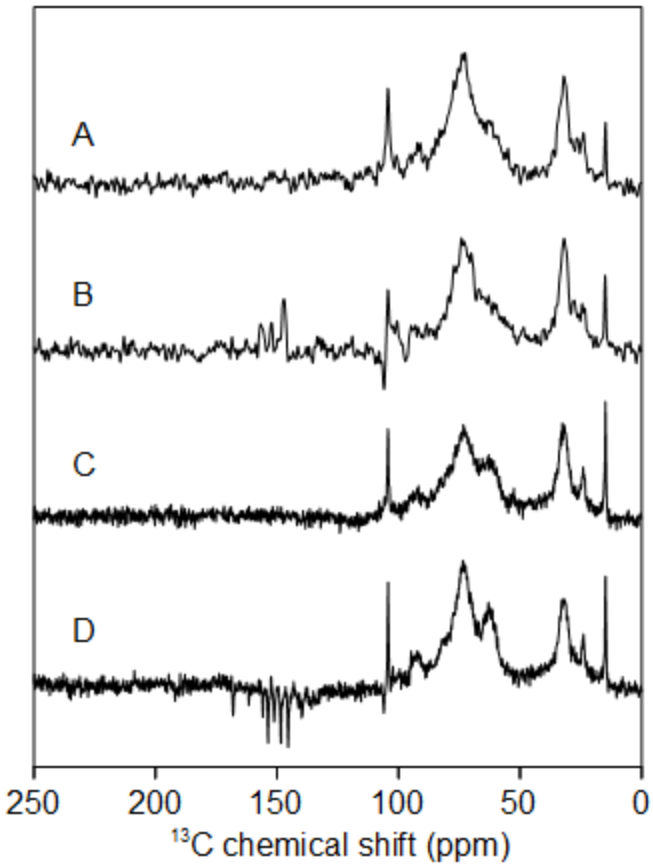

Figure 10: Magnetic field dependent ^{13}C MAS NMR spectra of PS II core complexes from *P. tricornutum*: A) dark spectrum at 4.7 T, B) light spectrum at 4.7 T, C) dark spectrum at 9.4 T, D) light spectrum at 9.4 T.

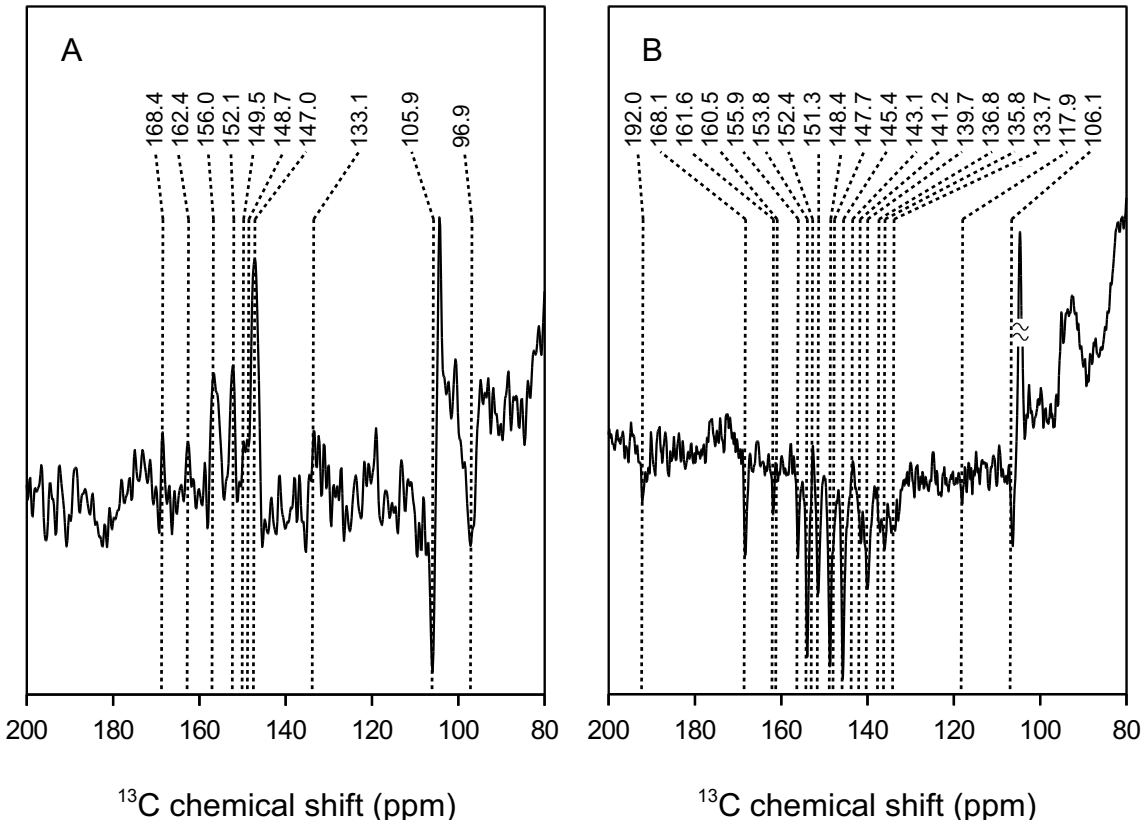

Figure 11: Zoom into the aromatic region of the ^{13}C photo-CIDNP MAS NMR spectra of PS II core complexes from *P. tricornutum* obtained at magnetic fields of A) 4.7 T and B) 9.4 T.

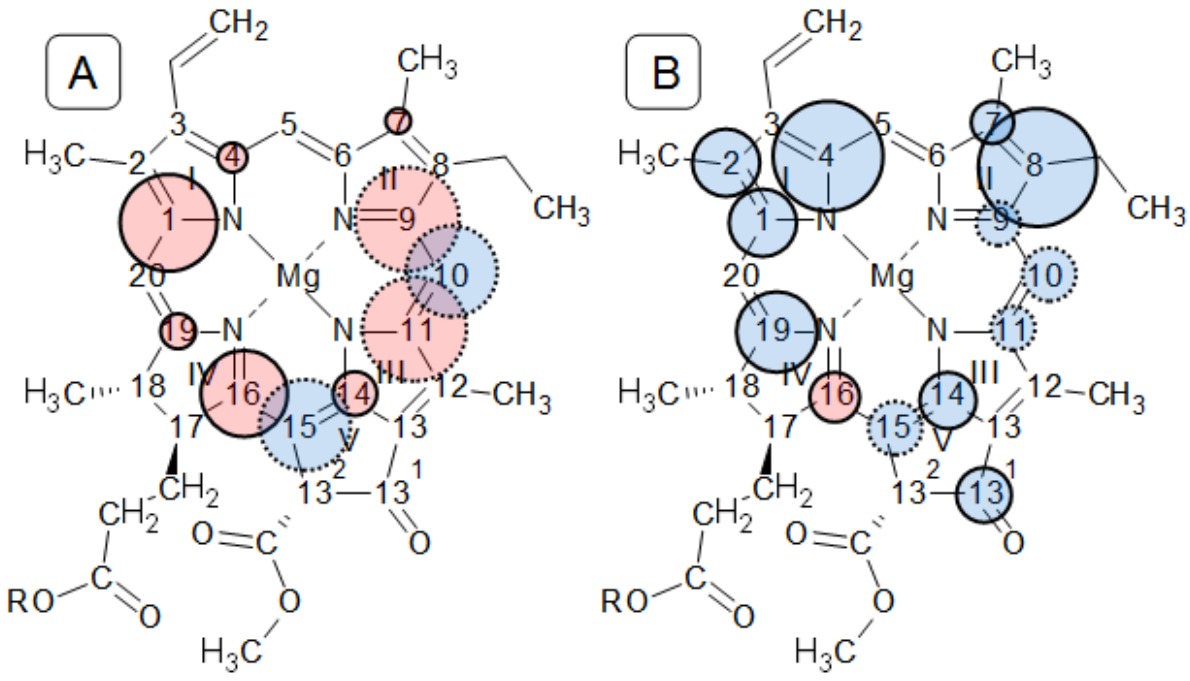

Figure 12: ^{13}C Photo-CIDNP patterns of the Chl *a* donor molecule of PS II core complexes isolated from *P. tricornutum* at different magnetic fields: A: 4.7 T and B: 9.4 T. The sizes of the circles depict the NMR intensities. Positions with absorptive polarisation are labelled in red, emissive signals are displayed in blue. Dashed circles represent carbons that might be assigned to two positions. R = Phytyl side chain.

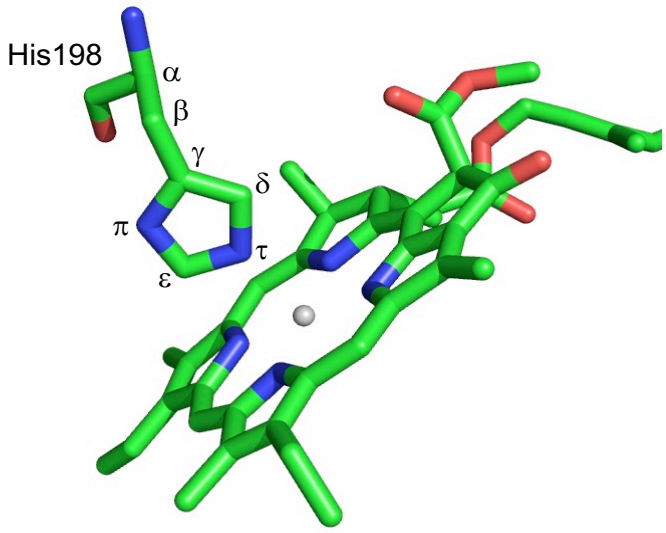

Figure 13: Detailed view on the Chl *a* donor of PS II of spinach and the histidine ligating from an axial position (3JCU.pdb) (Wei et al. 2013).

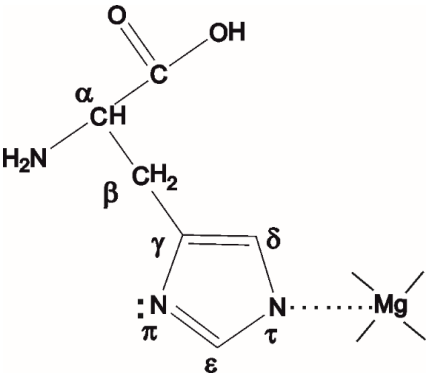

Scheme 2: ^{13}C and ^{15}N photo-CIDNP MAS NMR data show that the τ-N of histidine is ligating to the Mg^{2+} of the donor Chl *a* of PS II from *P. tricornutum*. It appears that the π-N has a lone pair.

Tab. 1: ^{15}N-chemical shifts of the photo-CIDNP MAS NMR signals compared to chemical shift data reported in the literature.

Cofactor	Atom	Solution data[a]	PSI/PSII fraction from *P. tricornutum*[b]	PS I from spinach at 9.4 T[c]	PS II from spinach at 4.7 T[c]
Chl *a*	N-I	186.0	186.0 (E)	186.2 (E)	
	N-I		190.8 (A)	190.9 (A)	
	N-II	206.5	213.4 (E)		211.5 (E)
	N-II		212.0 (E)	211.5 (E)	
	N-II		206.1 (A)	206.1 (A)	
	N-III	189.4	195.9 (E)		195.3 (E)
	N-III		198.8 (E)		
	N-III		193.1 (A)	193.2 (A)	
	N-IV	247.0	248.5 (E)		247.6 (E)
	N-IV		255.5 (E), 251.9 (E)	254.9 (E), 250.3 (E)	
	N-IV		233.5 (A)	233.3 (A)	
Phe *a*	N-I	125.5	-	-	
	N-II	241.5	243.7 (E)*	-	
	N-III	133.9	138.6 (E)	-	138.3 (E)
	N-IV	295.8	297.3 (E)	-	295.0 (E)
Histidine	π-N		243.7 (E)*		243.8 (E)
	τ-N		224.9 (E)	-	-

[a] solution data, measured in $CDCl_3$, ref. (Boxer et al. 1974).

[b] This work.

[c] PS I and PS II from spinach, ref. (Diller et al. 2007a).

* cannot be clearly assigned to one position.

Tab. 2: ^{13}C chemical shifts of the photo-CIDNP MAS NMR signals from PSI/PSII fractions of *P. tricornutum* compared to chemical shifts of Chl *a* and Phe *a* from the literature.

^{13}C chemical shift (ppm)[a]	Carbon atom	^{13}C chemical shift (ppm)[b]	^{13}C chemical shift (ppm)[c]	^{13}C chemical shift (ppm)[d]	^{13}C chemical shift (ppm)[e]	^{13}C chemical shift (ppm)[f]
192.1 (E)	13[1]	190.6	190	190.4 (E)		192.0 (E)
168.3 (E)	**19**	**170.0**	171	**166.6 (A)**	**166.8 (A)**	**168.2 (E)**
161.6 (E) br.	**14**	**162.0**		**162.1 (A)**	**162.2 (A)**	**161.7 (E)**
161.6 (E) br.	16		161	160.6(A)		
156.3 (E)	**1**	**155.9**		**156.0 (A)**	**156.0 (A)**	**156.1 (E)**
154.7 (E)	**6**	**154.4**		**155.0 (A)**	**154.6 (A)**	
153.8 (E)	6		156	153.9 (A)		
152.7 (A)	**16**	**154.0**		**157.5 (A)**	**151.6 (A)**	
151.1 (E)	14 and 4		151	151.5 (A)		
148.5 (E)	**4**	**150.7**		**148.8 (A)**	**149.2 (A)**	**151.2 (E)**
147.7 (E)	**9 and 11**	**147.2**		**147.2 (A)**	**147.2 (A)**	**148.4 (E) and**
				and 147.8 (A)		**147.8 (E)**
145.6 (E)	8	146.2	145	146.6 (A)	146.0 (A)	145.5 (E)
143.3 (A)	1		142			
142.5 (E)	His ?			142.5 (E,His ?)		
139.9 (E)	3			138.2 (A)	137.4 (A)	139.8 (E)
137.3 (E) br.	**2**	**136.1**			**136.0 (A,C-2)**	**137.9 (E)**
	and His (ε-C)			136.0 (A, His)		
133.4 (E)	**7**	**133.4**		-	**~132 (A)**	**133.4 (E) br.**
	and His (γ-C)					
118.2 (E)	His (δ-C)					

106.3 (E)	10 and 15	108.2 and 105 102.8 and107	104.8 (E) and 106.9 (E) and 105.9 (E) 103.9 (E) 104.7 (E)	

[a] This work, samples including both PSs of diatom *P. tricornutum* measured at 9.4 T.

[b] Isolated Chl *a* as solid aggregate (SDBS 1999).

[c] plant Phe *a* recomstituted in *R. sphaeroides* R26 RCs (Boender 1996).

[d] PS II thylakoids from duckweed, 4.7 T (Egorova-Zachernyuk et al. 1997).

[e] PS II from spinach, 9.4 T, ref. (Alia et al. 2004).

[f] PS I core complexes from *C. meneghiniana*, 9.4 T, ref. (Zill et al. 2017b).

br. = broad, His = histidine.

Tab. 3: Overview on the photo-CIDNP MAS NMR resonances of PS II core complexes from *P. tricornutum* at different magnetic fields.

^{13}C chemical shift (ppm)[a]	^{13}C chemical shift (ppm)[b]	Carbon atom	^{13}C chemical shift (ppm)[c]	^{13}C chemical shift (ppm)[d]	^{13}C chemical shift (ppm)[e]	^{13}C chemical shift (ppm)[f]
	192.0 (E)	13[1]	190.6	190	190.4 (E)	
168.4 (A)	168.1 (E)	19	170.0	171	166.6 (A)	166.8 (A)
162.4 (A)	**161.6 (E)**	**14**	**162.0**		**162.1 (A)**	**162.2 (A)**
	(160.5 (E))	16		161	160.6(A)	
156.0 (A)	**155.9 (E)**	**1**	**155.9**		**156.0 (A)**	**156.0 (A)**
(156.0 (A))	153.8 (E) br.	6		156	153.9 (A)	
152.1 (A)	**152.4 (A)**	**16**	**154.0**		**157.5 (A)**	**151.6 (A)**
	151.3 (E) br.	14		151	151.5 (A)	
149.5 (A)	**148.4 (E)**	**4**	**150.7**		**148.8 (A)**	**149.2 (A)**
148.7 (A) and	**147.7 (E)**	**9 and 11**	**147.2**		**147.2 (A) and**	**147.2 (A)**
147.0 (A)					**147.8 (A)**	
	145.4 (E)	8	146.2	145	146.6 (A)	146.0 (A)
	143.1 (A)	1		142	142.3 (A)	
	141.2 (E)	His?			142.5 (E)	
	139.7 (E) br.	3		136	138.2(A)	137.4 (A)
	136.8 (E)	His (ε-C)			136.0 (E)	
	135.8 (E)	**2**	**136.1**			**136.0 (A)**
133.1 (A)	**133.7 (E)**	**7 and**	**133.4**			**~132 (A)**
		His (γ-C)				
	117.9 (E)	His (δ-C)				
105.8 (E)	106.1 (E)	10 and 15	108.2 and	105 and	104.8 (E) and	
			102.8	107	103.9 (E)	

96.9 (E)		5	98.1	97	97.9 (E)	97.9 (E)

[a] This work, PS II core complexes from *P. tricornutum* measured at 4.7 T, [b] This work, PS II core complexes from *P. tricornutum* measured at 9.4 T. [c] Isolated Chl *a* as solid aggregate (SDBS 1999), [d] plant Phe *a* reconstituted in *R. sphaeroides* R26 RCs (Boender 1996). [e] PS II thylakoids from duckweed, 4.7 T (Egorova-Zachernyuk et al. 1997), [f] PS II D1D2 preparation from spinach 9.4 T (Alia et al. 2004). His = histidine, bold = assigned to Chl *a* only, br. = broad (>70 Hz).

Tab. 4: ^{13}C and ^{15}N Photo-CIDNP MAS NMR signals attributed to histidine.

Histidine position	chemical shift (ppm)					
	neutral histidine without π-N-H-bonding[a]	neutral histidine with π-N-H-bonding[a]	neutral histidine with π-N-H-bonding, no Mg^{2+} ligation[b]	cationic histidine with lonepair at the π-N[b]	*P. tricornutum*	photo-CIDNP in Literature
γ-C	-	-	137.0	128.0	133.7[c](133.4[d])	134.2 (A)[e]
δ-C	121.9	119.1	113.5	119.3	117.9[c](118.2[d])	
ε-C	130.9	129.9	138.6	136.4	136.8[c](137.3[d])	136.0 (A)[e]
π-N	170	175	250	178	243.7 (E)[d]	243.8 (E)[f]
τ-N	225	220	176	225	224.9 (E)[d]	

[a] data from Alia et al. 2001.

[b] data from Nagao et al. 2009.

[c] this work, data from PS II from *P. tricornutum*.

[d] this work, data from PSI/PSII fraction from *P. tricornutum.*

[e] data from Egorova-Zachernyuk et al. 1997.

[f] data from Prakash et al. 2005b.